ANTIOXIDANTS & REDOX SIGNALING
Volume 21, Number 12, 2014

DOI: 10.1089/ars.2013.5479

ORIGINAL RESEARCH COMMUNICATION

Membrane-Bound CYB5R3 Is a Common Effector of Nutritional and Oxidative Stress Response Through FOXO3a and Nrf2

Emilio Siendones,[1,2] Sara SantaCruz-Calvo,[1,2] Alejandro Martín-Montalvo,[3] María V. Cascajo,[1,2] Julia Ariza,[4] Guillermo López-Lluch,[1,2] José M. Villalba,[4] Cécile Acquaviva-Bourdain,[5] Emmanuel Roze,[6] Michel Bernier,[3] Rafael de Cabo,[3] and Plácido Navas[1,2]

Abstract

Aims: Membrane-bound CYB5R3 deficiency in humans causes recessive hereditary methaemoglobinaemia (RHM), an incurable disease that is characterized by severe neurological disorders. *CYB5R3* encodes for NADH-dependent redox enzyme that contributes to metabolic homeostasis and stress protection; however, how it is involved in the neurological pathology of RHM remains unknown. Here, the role and transcriptional regulation of *CYB5R3* was studied under nutritional and oxidative stress. ***Results:*** *CYB5R3*-deficient cells exhibited a decrease of the NAD^+/NADH ratio, mitochondrial respiration rate, ATP production, and mitochondrial electron transport chain activities, which were associated with higher sensitivity to oxidative stress, and an increase in senescence-associated β-galactosidase activity. Overexpression of either forkhead box class O 3a (FOXO3a) or nuclear factor (erythroid-derived 2)-like2 (Nrf2) was associated with increased CYB5R3 levels, and genetic ablation of Nrf2 resulted in lower CYB5R3 expression. The presence of two antioxidant response element sequences in the *CYB5R3* promoter led to chromatin immunoprecipitation studies, which showed that cellular stressors enhanced the binding of Nrf2 and FOXO3a to the *CYB5R3* promoter. ***Innovation:*** Our findings demonstrate that *CYB5R3* contributes to regulate redox homeostasis, aerobic metabolism, and cellular senescence, suggesting that *CYB5R3* might be a key effector of oxidative and nutritional stress pathways. The expression of CYB5R3 is regulated by the cooperation of Nrf2 and FOXO3a. ***Conclusion:*** *CYB5R3* is an essential gene that appears as a final effector for both nutritional and oxidative stress responses through FOXO3a and Nrf2, respectively, and their interaction promotes CYB5R3 expression. These results unveil a potential mechanism of action by which CYB5R3 deficiency contributes to the pathophysiological underpinnings of neurological disorders in RHM patients. *Antioxid. Redox Signal*. 21, 1708–1725.

Introduction

CYB5R3 ENCODES FOR a NADH-cytochrome b_5 reductase 3 (NADH:ferricytochrome b_5 oxidoreductase, EC1.6.2.2), a flavoprotein that catalyzes electrons transfer from NADH to cytochrome b_5 or to plasma membrane coenzyme Q, producing cytosolic NAD^+ (37, 47). *CYB5R3* encodes for two isoforms: a soluble one, exclusively expressed in erythrocytes, and a membrane-bound isoform anchored to the mitochondrial outer membrane, endoplasmic reticulum, and plasma membrane. *CYB5R3* deficiency causes a rare recessive hereditary methaemoglobinaemia (RHM). Type I RHM

[1]Centro Andaluz de Biología del Desarrollo, Universidad Pablo de Olavide-CSIC-JA, Sevilla, Spain.
[2]Centre for Biomedical Research on Rare Diseases (CIBERER), ISCIII, E-41013 Sevilla, Spain.
[3]Translational Gerontology Branch, National Institute on Aging, NIH, Baltimore, Maryland.
[4]Departamento de Biología Celular, Fisiología e Immunología, Universidad de Córdoba, Córdoba, Spain.
[5]Service des Maladies Héréditaires du Métabolisme et Depistage Neonatal, Centre de Biologie et de Pathologie, Lyon, France.
[6]Centre de Recherche de l'Institut du Cerveau et de la Moelle épinière (CRICM), INSERM U975, CNRS UMR 7225, UPMC Université Paris 6 UMR_S 975, Paris, France.

Innovation

NADH-cytochrome b_5 reductase 3 contributes to metabolic homeostasis and stress protection in cellular membranes. Our study describes novel roles of the membrane-bound *CYB5R3* in the regulation of redox homeostasis, aerobic metabolism, and in protection against cellular senescence. We established that both serum withdrawal and hydrogen peroxide treatment induced cooperation between nuclear factor (erythroid-derived 2)-like2 (Nrf2) and FOXO3a to regulate *CYB5R3* transcription. The control of aerobic metabolism and cytosolic NAD^+/NADH ratio by CYB5R3 provides a key regulatory function in the maintenance of cellular health and contributes a new approach to understanding the pathophysiology of recessive hereditary methaemoglobinaemia and other disorders associated with energy depletion and oxidative stress.

is benign, limited to the soluble isoform in erythrocytes (15, 45); whereas type II RHM affects all cells, is incurable, and is characterized by severe neurological disorders (15, 45, 47). Membrane-bound CYB5R3 acts in elongation and unsaturation of fatty acids (44), cholesterol biosynthesis (52), and drug metabolism (19, 57). Furthermore, *CYB5R3* is induced under stress conditions and maintains antioxidants, such as coenzyme Q, α-tocopherol, and ascorbate, in their reduced form, thereby conferring protection against lipid peroxidation (7, 12, 13). CYB5R3 expression and activity is also induced by calorie restriction, which might prevent the accumulation of oxidative stress damage with age (38). These latter functions, mainly associated to plasma membrane, are essential to sustain the cytosolic redox homeostasis in ρ° cells (cells lacking mitochondrial genome) (22). In yeast, the plasma membrane NADH-coenzyme Q reductase 1 (*NQR1*), an orthologue of mammalian *CYB5R3*, uses NADH and coenzyme Q_6 as substrates, induces a shift from fermentation to respiration, and contributes to extend both chronological and replicative life span (23).

Environmental stressors play a role in the development of cancer, neurodegenerative diseases, and other age-related diseases (16, 28, 60). The nuclear factor (erythroid-derived 2)-like2 (Nrf2) and the forkhead box class O 3a (FOXO3a) are two emerging regulators of cellular redox homeostasis. Nrf2 binds to the antioxidant response elements (ARE) that are present in the promoter of more than 200 genes encoding for antioxidant enzymes such as NAD(P)H:quinone oxidoreductase 1 (*NQO1*) (34, 40, 58, 39). Recently, it has been shown that the deletion of Nrf2 decreased lifespan of mouse embryonic fibroblasts (MEFs) (24), and blunted the protective effect of calorie restriction against cancer (46). Moreover, the silencing of Nrf2 leads to premature senescence; whereas several Nrf2 inducers enhanced survival and lifespan of cultured human fibroblasts (26). AKT-mediated regulation of FOXO3a activity contributes to redox signaling, metabolism, and longevity (4, 10, 14, 18, 53, 59, 66, 67). FOXO3a activity is required to ameliorate oxidative stress damage during erythropoiesis (33) and in the protection against oxidative stress-induced cell death by up-regulation of the mitochondrial superoxide dismutase and peroxiredoxin III (11). The antioxidant defense provided by FOXO family members, such a FOXO3a, is now recognized as an anti-aging mechanism that regulates redox signaling and ameliorates mitochondrial oxidative stress production during aerobic metabolism (3, 10, 14, 55, 58).

In this article, we set out to investigate the role of *CYB5R3* in the maintenance of sustained respiratory metabolism, stress protection, and *in vitro* cell senescence. We also investigated the role of Nrf2 and FOXO3a in the induction of *CYB5R3* under diverse stress conditions.

Results

CYB5R3 deficiency results in decreased growth and early senescent phenotype

To study the importance of *CYB5R3* in the control of cellular homeostasis, we used human dermal fibroblasts (HDF) from two patients (5- and 22 months old) with type II RHM, harboring mutations in the *CYB5R3* gene that result in the lack of CYB5R3 enzymatic activity (Fig. 1A). CYB5R3 protein was not detected in patient 1, perhaps because it was unstable; while in patient 2, a small-sized peptide was detected, probably due to the generation of a truncated CYB5R3 isoform. After several passages, both cell lines exhibited a flattened morphology and an enlargement of their cytoplasm with increased staining for the senescence-associated β-galactosidase (SA-β-gal) when compared with neonatal HDFs at similar passages (Fig. 1A).

The difficulty to transfect HDFs from patients led us to use the HDF cell line MRC-5 for various genetic manipulation experiments that are aimed at assessing the physiological role of CYB5R3. These cells were found to be efficiently transfected with plasmids and siRNAs as shown next.

Three different siRNAs targeting *CYB5R3* were introduced in ''young'' MRC-5 cells at < 35 population doublings (PDs). siRNA transfection was carried out for 48–72 h, after which CYB5R3 mRNA and protein levels were determined. A significant and sustained decrease in CYB5R3 expression (85% or greater) was observed during the first three passages (Fig. 1B). *CYB5R3*-silenced MRC-5 cells exhibited a slower proliferation rate as compared with cells transfected with control nonsilencing siRNA (Fig. 2A). However, these cells did not stain strongly for SA-β-gal activity, unlike HDFs from patients. Interestingly, the introduction of siRNAs in ''aged'' MRC-5 cells (> 50 passages, > 65 PDs) significantly increased the percentage of cells showing positive SA-β-gal stain (Fig. 2B).

CYB5R3 is involved in aerobic metabolism

The maintenance of an optimal NAD^+/NADH ratio is essential for cellular and metabolic homeostasis (48). The role of CYB5R3 in modulating pyridine nucleotides redox state and mitochondrial function was then assessed in *CYB5R3*-silenced MRC-5 cells. The NAD^+/NADH ratio was drastically decreased on CYB5R3 down-regulation (Fig. 3A) but not the nicotinamide phosphoribosyltransferase (NAMPT) mRNA and total NAD (defined as the amount of NADH + NAD^+) levels (Supplementary Fig. S1; Supplementary Data are available online at www.liebertpub.com/ars). The silencing of *CYB5R3* was accompanied by a significant decrease of mitochondrial respiration, as measured by cyanide-sensitive oxygen consumption (Fig. 3B).

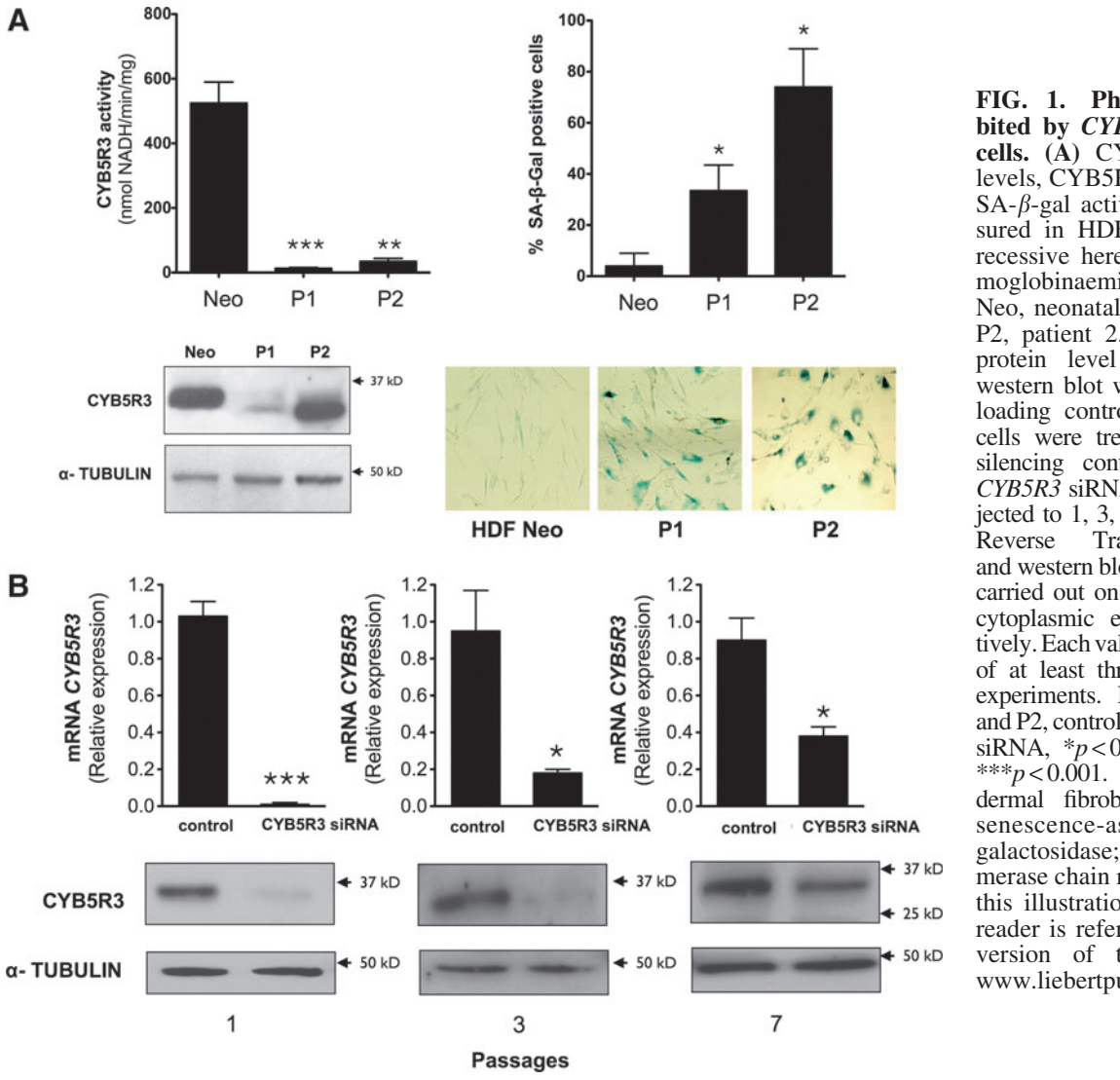

FIG. 1. Phenotype exhibited by *CYB5R3*-defective cells. **(A)** CYB5R3 protein levels, CYB5R3 activity, and SA-β-gal activity were measured in HDF from type II recessive hereditary methaemoglobinaemia patients. Neo, neonatal; P1, patient 1; P2, patient 2. The α-tubulin protein level evaluated by western blot was used as the loading control. **(B)** MRC-5 cells were treated with non-silencing control siRNA or *CYB5R3* siRNA and then subjected to 1, 3, and 7 passages. Reverse Transcriptase-PCR and western blot analyses were carried out on total RNA and cytoplasmic extracts, respectively. Each value is mean $\pm$ SD of at least three independent experiments. Neo *versus* P1 and P2, control *versus CYB5R3* siRNA, $*p<0.05$, $**p<0.01$, $***p<0.001$. HDF, human dermal fibroblast; SA-β-gal, senescence-associated β-galactosidase; PCR, polymerase chain reaction. To see this illustration in color, the reader is referred to the web version of this article at www.liebertpub.com/ars

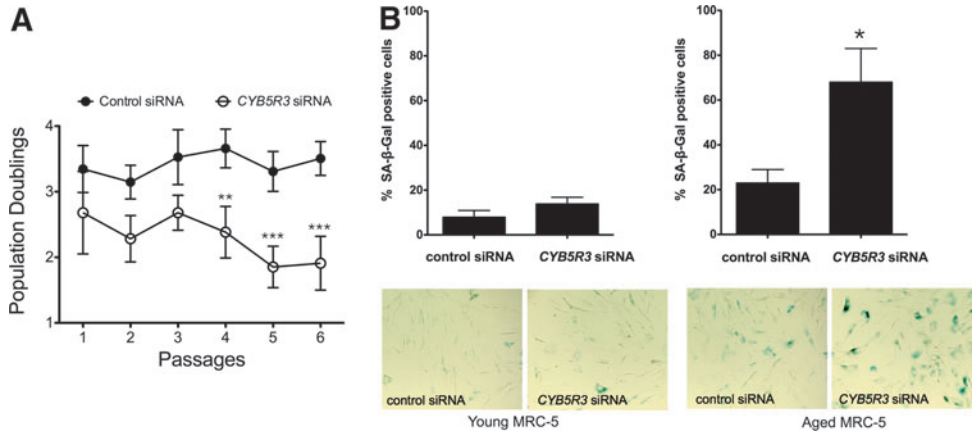

FIG. 2. Growth and senescent phenotype exhibited by *CYB5R3*-defective cells. **(A)** Population doublings of control- (●) and *CYB5R3* siRNA-treated (○) MRC-5 cells. **(B)** SA-β-gal activity was measured in young and aged MRC-5 cells that were treated with either control or *CYB5R3* siRNA. Each value is mean $\pm$ SD of at least three independent experiments. Control *versus CYB5R3* siRNA, $*p<0.05$, $**p<0.01$, and $***p<0.001$. To see this illustration in color, the reader is referred to the web version of this article at www.liebertpub.com/ars

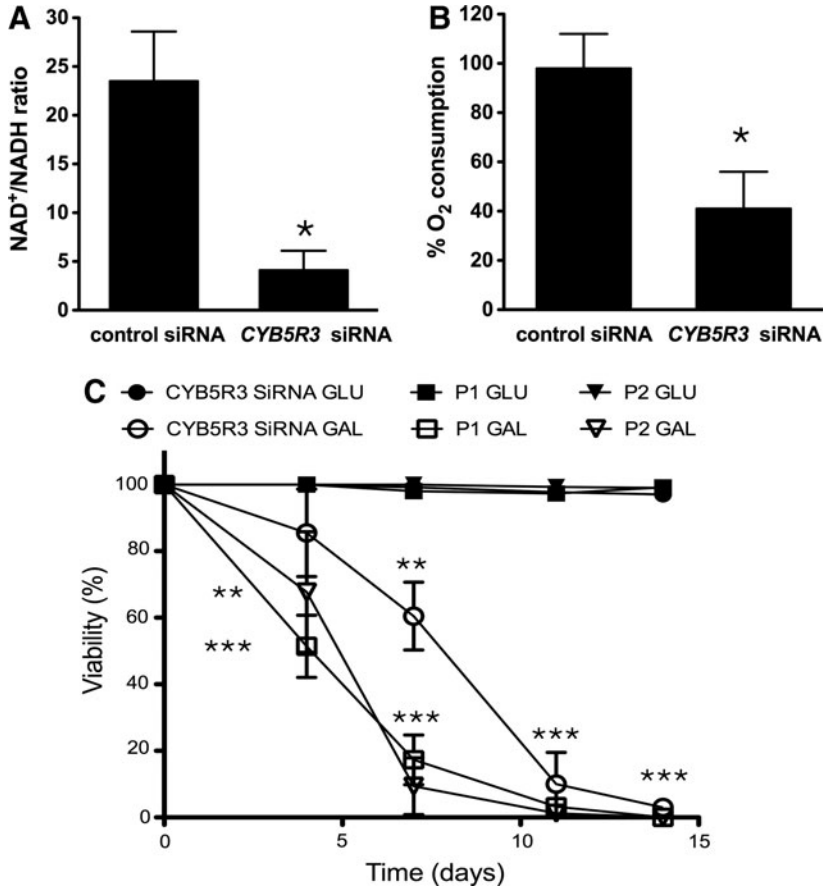

FIG. 3. CYB5R3 activity modulates the cytoplasmic ratio of pyridine nucleotides and oxygen consumption. **(A)** Decreased cytoplasmic NAD^+/NADH ratio and **(B)** cyanide-sensitive O_2 consumption in *CYB5R3*-silenced MRC-5 cells. **(C)** MRC-5 cells with transient siRNA-mediated *CYB5R3* knockdown and HDF from patients P1 and P2 were cultured for 14 days in medium that was supplemented with either 25 m*M* glucose (GLU) or galactose (GAL). Cell viability was determined every 3–4 days for 14 days. Each value is mean ± SD of at least three independent experiments. Control *versus CYB5R3* siRNA, GLU- *versus* GAL-based medium $*p < 0.05$, $**p < 0.01$, $***p < 0.001$.

The oxidation of galactose to pyruvate *via* glycolysis does not yield net ATP (1), and cells cultured with this carbon source are forced to produce energy through oxidative phosphorylation (34, 54, 56), making them very sensitive to mitochondrial dysfunction. Primary skin fibroblasts from patients with defects in the respiratory chain complexes, coenzyme Q deficiency, or pyruvate dehydrogenase deficiency have poor survivability in galactose-based medium (1, 49, 50). Compared with their respective controls, both *CYB5R3*-silenced MRC-5 cells and type II RHM HDFs displayed a low proliferation rate and increased cell death when maintained in galactose-based medium (Fig. 3C), which is consistent with possible impairment in mitochondrial metabolism.

The impact of CYB5R3 on various bioenergetic endpoints, including mitochondrial oxygen consumption, lactate production, ATP levels, and electron transport respiratory chain activities, was then assessed. In the first series of experiments, cellular respiration was measured as an index of mitochondrial function using the Seahorse Bioscience XF analyzer with a stable MRC-5 cell line expressing *CYB5R3*-specific shRNA (MRC-5/*CYB5R3* shRNA) and HDFs from patients with RHMII. Oxygen consumption rates (OCR) of MRC-5/*CYB5R3* shRNA and patient HDFs-cultured cells are shown in Figure 4A and B, respectively. Results show mitochondrial respiratory response before and after the sequential addition of oligomicin (OL) and 2,5 dinitrophenol (DNP) to the cells. MRC-5/*CYB5R3* shRNA cells and patients' HDFs cultured under standard conditions had basal respiration (BR) that was lower than that for their control counterparts (Fig. 4A, B). Treatment with the mitochondrial uncoupler DNP caused an increase in the OCR of cells. Both MRC-5/*CYB5R3* shRNA cells and patients' HDFs failed to achieve maximal respiration response observed in control cells after DNP treatment and also exhibited a reduced spare respiratory capacity (SRC) (Fig. 4A, B). The increased lactate production in patients' HDFs (Fig. 5A, right graph) was associated with lower intracellular ATP levels (Fig. 5B, right graph) through significant impairment in mitochondrial respiratory chain enzymatic activities (complexes I–IV) (Fig. 5C, right graph). Similarly, *CYB5R3*-silenced MRC-5 cells had a significant decrease of intracellular ATP levels (Fig. 5B, left graph) and also exhibited a significant decrease of the activities of the respiratory chain (Fig. 5C, left graph).

Upregulation of CYB5R3 in serum-deprived and diquat-stimulated cells

Given the antioxidant properties of CYB5R3, we hypothesized that CYB5R3 gene expression could be transcriptionally regulated by FOXO3a and Nrf2. Inactivation of the phosphatidylinositol-4,5-bisphosphate 3-kinase (PI3K)/AKT pathway by serum deprivation elicits the translocation of active (e.g., dephosphorylated) FOXO3a to the nucleus (10, 27, 11, 58). To assess the expression levels of CYB5R3 under serum deprivation, the culture medium of 3 confluent HDF cell lines was replaced with serum-free medium (SFM) for 30–48 h. Proliferating cells were obtained by reseeding HDF cells at a low density in fresh medium with serum. Western blot analysis of cytoplasmic extracts indicated that the

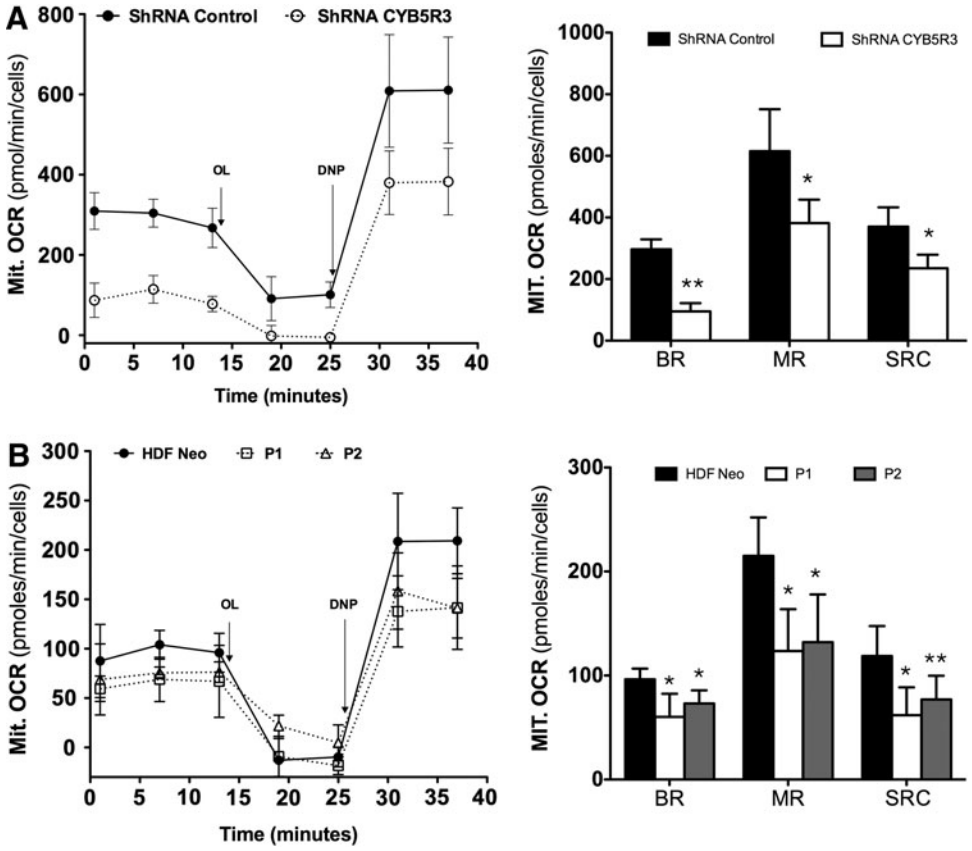

FIG. 4. CYB5R3 activity modulates mitochondrial respiration. (A, B) Mit. OCR after the sequential addition of oligomycin A, 2,5-dinitrophenol to MRC-5 cells that were stably transfected with *CYB5R3* shRNA **(A,** *left panel*) and HDFs from patients P1 and P2 **(B,** *left panel*). **(A** and **B,** *right panels*): Quantification of the mitochondrial BR, MR, and SRC. These parameters were calculated as described in Materials and Methods. Each value is mean ± SD of five independent experiments. shRNA control *versus CYB5R3* shRNA, HDF neo *versus* P1 and P2. $*p < 0.05$, $**p < 0.01$. Mit. OCR, mitochondrial oxygen consumption rates; BR, basal respiration; SRC, spare respiratory capacity; MR, maximal respiration.

CYB5R3 protein levels were highly increased in serum-deprived HDFs and that this effect was associated with AKT inactivation and concomittant reduction in phospho-FOXO3a levels (Fig. 6). The importance of the PI3K/AKT pathway in the control of CYB5R3 expression was assessed by incubating serum-deprived HDFs with the pharmacological inhibitor LY294002 (Fig. 7). A 30-h stimulation with insulin markedly blocked the expression of CYB5R3 mRNA and protein induced by serum depletion, and pretreatment with LY294002 abrogated this insulin response (Fig. 7A). Under these conditions, the ability of insulin to prevent SFM-dependent activation of FOXO3a through dephosphorylation on Thr-32 was hindered by LY294002 pretreatment (Fig. 7B), indicating the exquisite control of CYB5R3 expression by AKT signaling.

The expression of CYB5R3 mRNA and protein was also increased in serum-deprived MRC-5 cells (Fig. 8A) in concomittant with a reduction in phospho-AKT levels. MRC-5 cells transfected with an FOXO3a expression plasmid exhibited a strong nuclear accumulation of exogenous FOXO3a in response to serum depletion (Fig. 8A). HeLa and HepG2 cells, which had relatively low levels of CYB5R3, responded to LY294002 treatment with increased expression of CYB5R3 protein and a larger pool of dephosphorylated (activated) FOXO3a (Supplementary Fig. S2). We also evaluated the mitochondial respiration when FOXO3a is activated by SFM. Serum-deprived cells significantly increased cyanide-sensitive oxygen consumption as compared with cells maintained in complete medium. However, no increase of oxygen consumption was observed in MRC-5/*CYB5R3* shRNA cells maintained in SFM (Supplementary Fig. S3). To further examine the role of AKT in the control of *CYB5R3* expression, MRC-5 cells were transfected with an expression plasmid encoding a constitutively active form of AKT (N-myristoylated). These cells exhibited lower CYB5R3 levels and a marked inactivation of FOXO3a (phosphorylated) under serum deprivation (Supplementary Fig. S4). These results confirmed the requirement for AKT inactivation in the induction of *CYB5R3* expression.

Diquat activates Nrf2 (Supplementary Fig. S5) through the superoxide generation in mitochondria (43, 68, 69). The exposure of MRC-5 cells to diquat significantly increased the expression of CYB5R3 mRNA and protein (Fig. 8B). To ascertain the direct role of Nrf2 in *CYB5R3* expression, wild-type and $Nrf2^{-/-}$ MEFs were treated with and without diquat, and CYB5R3 expression was evaluated (Fig. 8B). As shown earlier with MRC-5 cells, diquat-treated wild-type MEFs had higher levels of CYB5R3 mRNA and protein as compared with untreated control cells; however, $Nrf2^{-/-}$ MEFs exhibited lower basal levels of *CYB5R3*, and they were refractory to diquat exposure (Fig. 8B). To explore a possible relationship between FOXO3a and Nrf2 in the regulation of CYB5R3 expression, the levels of FOXO3a phosphorylation were determined by western blotting in serum-deprived MEFs. There was no reduction in phospho-FOXO3a levels in $Nrf2^{-/-}$ cells *versus* wild-type MEFs after serum withdrawal (Fig. 8B, bottom panel), suggesting that Nrf2 is required for FOXO3a activation (dephosphorylation). Ponceau staining of nitocellulose membranes after protein transfer was performed to demonstrate equal protein load in each lane (Supplementary Fig. S6).

CYB5R3 protects against oxidative stress

To explore the role of CYB5R3 in the defense against oxidative stress, viability of MRC-5 cells was determined

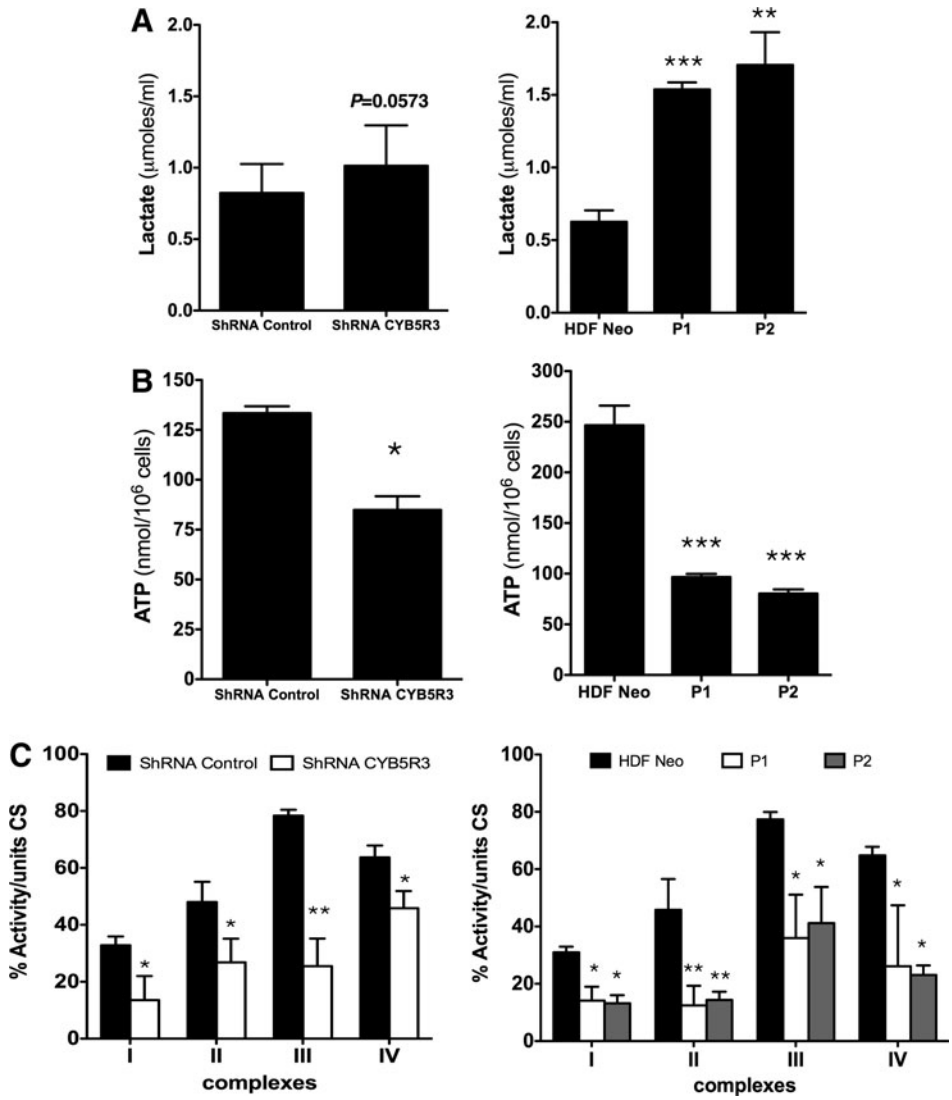

FIG. 5. Lactate and ATP levels and respiratory chain activities in *CYB5R3*-defective cells. (A) Lactate production and **(B)** ATP levels in MRC-5 cells stably transfected with *CYB5R3* shRNA and HDFs from patients P1 and P2. **(C)** Respiratory chain enzymatic activities of complexes I, II, III, and IV relative to citrate synthase. Values are means ± SD of three independent experiments. shRNA control *versus CYB5R3* shRNA, HDF neo *versus* P1 and P2. $*p < 0.05$, $**p < 0.01$, $***p < 0.001$.

after exposure to hydrogen peroxide (H_2O_2). Cells undergoing active proliferation exhibited a higher sensitivity to H_2O_2-mediated cell death than serum-deprived cells (Fig. 9A). The silencing of CYB5R3 rendered MRC-5 cells more sensitive to cell death in response to H_2O_2 as compared with cells transfected with a nonsilencing siRNA control (Fig. 9B). Similar results were obtained when control and *CYB5R3*-silenced MRC-5 cells were treated with diquat (Fig. 9C). The resistance of serum-deprived cells to diquat was not observed when MRC-5 cells were transfected with *CYB5R3*

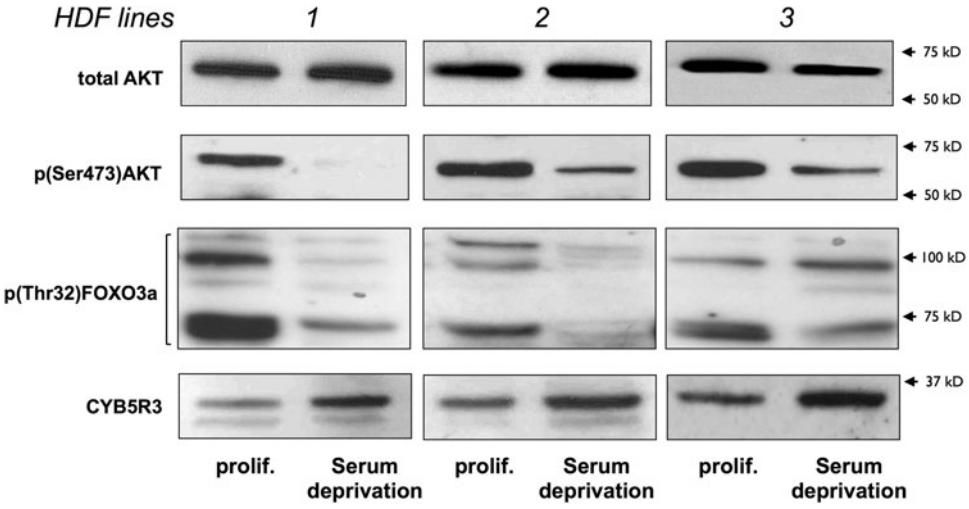

FIG. 6. Effect of absence of growth factors on *CYB5R3* expression. Three different HDF lines were cultured under control conditions and serum deprivation for 12 h. Cytoplasmic extracts were immunoblotted with primary antibodies that were raised against phospho-AKT, phospho-FOXO3a, CYB5R3, and total AKT, which served as a loading control. Figure is representative of three independent experiments. FOXO3a, forkhead box class O 3a; AKT, v-akt murine thymoma viral oncogene homolog 1.

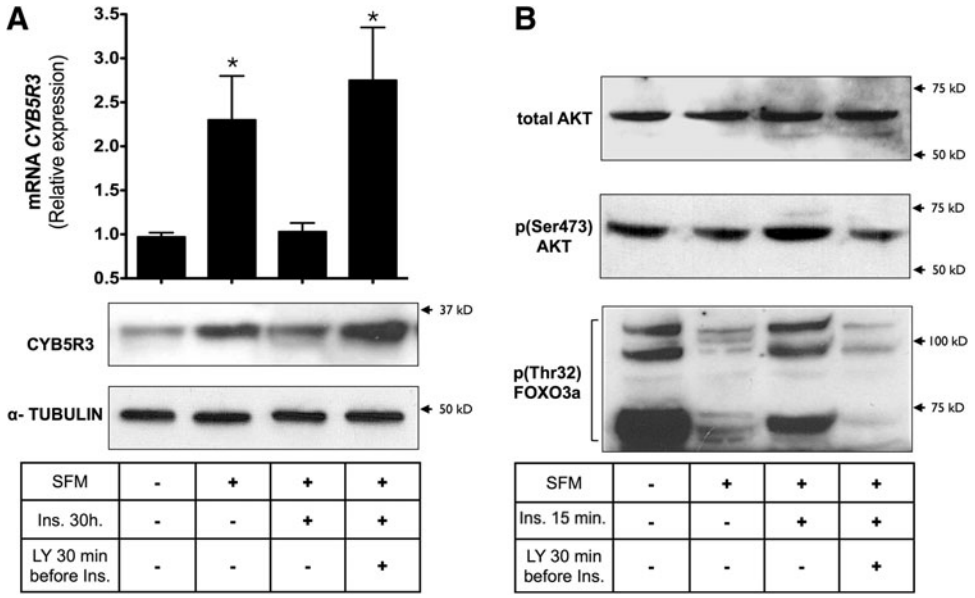

FIG. 7. Activation of AKT by insulin inhibits *CYB5R3* expression. **(A)** Serum-starved (SFM) HDF cells (line 1) were treated with insulin (100 n*M*) for 30 h to determine the *CYB5R3* mRNA and proteins levels. **(B)** In a second set of experiments, insulin was added for 15 min only to assess phosphorylation of AKT and FOXO3a. Groups of cells were pretreated with LY294002 (LY, 10 μM) for 30 min before the addition of insulin. Values are means ± SD of at least three independent experiments. Signals associated with AKT and α-tubulin served as loading controls. Control *versus* serum deprivation, insulin *versus* insulin + LY, $*p < 0.05$. SFM, serum-free medium.

siRNA, indicating that CYB5R3 confers protection against diquat (Fig. 9C).

Role of transcription factors FOXO3a and Nrf2 in the induction of CYB5R3

To determine whether activated FOXO3a contributes to the induction of CYB5R3, MRC-5 cells were transiently transfected with a plasmid encoding a mutated form of the human FOXO3a, which contains three alanine substitutions (A3 mutant) at the AKT phosphorylation sites, and fused to the ligand-binding domain of the estrogen receptor (FOXO3a-A3-ER). This construct is constitutively active by virtue of its protection against AKT-mediated phosphorylation. Under basal conditions, FOXO3a-A3-ER is located in the cytosol, but treatment with 4-hydroxytamoxifen (4-OHT) translocates FOXO3a into the nucleus (26) (Fig. 10A). Treatment with 4-OHT to cells overexpressing FOXO3a-A3-ER increased CYB5R3 protein levels and activity (Fig. 10B). The role of other FOXO members in the regulation of CYB5R3 expression was explored in HeLa cells overexpressing FOXO1-A3, FOXO4-A3, or FOXO3a-A3, which was used as control. Western blot analysis illustrated that neither FOXO1 nor FOXO4 stimulated the expression of *CYB5R3* (Supplementary Fig. S7).

Similarly, the overexpression of myc-tagged Nrf2 led to higher levels of CYB5R3 protein and activity in MRC-5 cells (Fig. 11A, B).

Nrf2 binds two sites of the CYB5R3 promoter

Human and mouse *CYB5R3* (22q13.2, 15 E;15 39.4, respectively) of the nonerythroid cells encode for a membrane-bound isoform that exhibits an additional exon (M) upstream of the first exon of the soluble protein present in erythrocytes. We performed an *in silico* analysis of the M exon sequence of human and mouse *CYB5R3* promoters and detected several putative ARE sites (Fig. 12 and Supplementary Fig. S8). Two specific primer pairs encompassing the regions at −1007/−851 bp (site 1) and −490/−1 bp (site 2) from the transcription start site of the human *CYB5R3* promoter were generated (Fig. 12). Chromatin immunoprecipitation (ChIP) analysis was performed, by which the Nrf2 immunoprecipitates were subjected to polymerase chain reaction (PCR) amplification with site 1 and site 2 primer pairs. The stimulation of MRC-5 cells with either diquat or serum deprivation increased the recruitment of Nrf2 to the *CYB5R3* promoter at sites 1 and 2 (Fig. 13A, B). Due to the lack of consensus sequences for FOXO3a binding in the exon M of *CYB5R3* promoter, we hypothesized that FOXO3a may interact with Nrf2 that is bound to sites 1 and 2 of the *CYB5R3* promoter. Using FOXO3a immunoprecipitates in ChIP assay, PCR amplification of sites 1 and 2 was observed under basal conditions (Fig. 14A). Lastly, western blotting of Nrf2 immunoprecipitates with anti-FOXO3a antibody confirmed the constitutive and inducible interaction between the two transcription factors (Fig. 14B).

Discussion

In this article, we show that CYB5R3 contributes to maintain respiratory metabolism, oxidative stress protection and prevents cell senescence. The induction of CYB5R3 gene expression is mediated by the coordinate action of Nrf2 and FOXO3a as a response to environmental stressors and starvation. These results unveil the existence of a mechanism that regulates the expression of *CYB5R3,* an essential gene in mammals, and indicate the orchestration of nutrient and oxidative stress response pathways to sustain cellular homeostasis.

Recent results have shown that increased CYB5R3 activity in plasma membrane of rat brain under caloric restriction and in rat neuronal cells grown in medium supplemented with serum from calorie restricted animals confers protection against oxidative stress in aging (21). *CYB5R3* is associated with lipid rafts at the plasma membrane of cerebellar granule neurons, playing a role at the interneuronal contact sites (2).

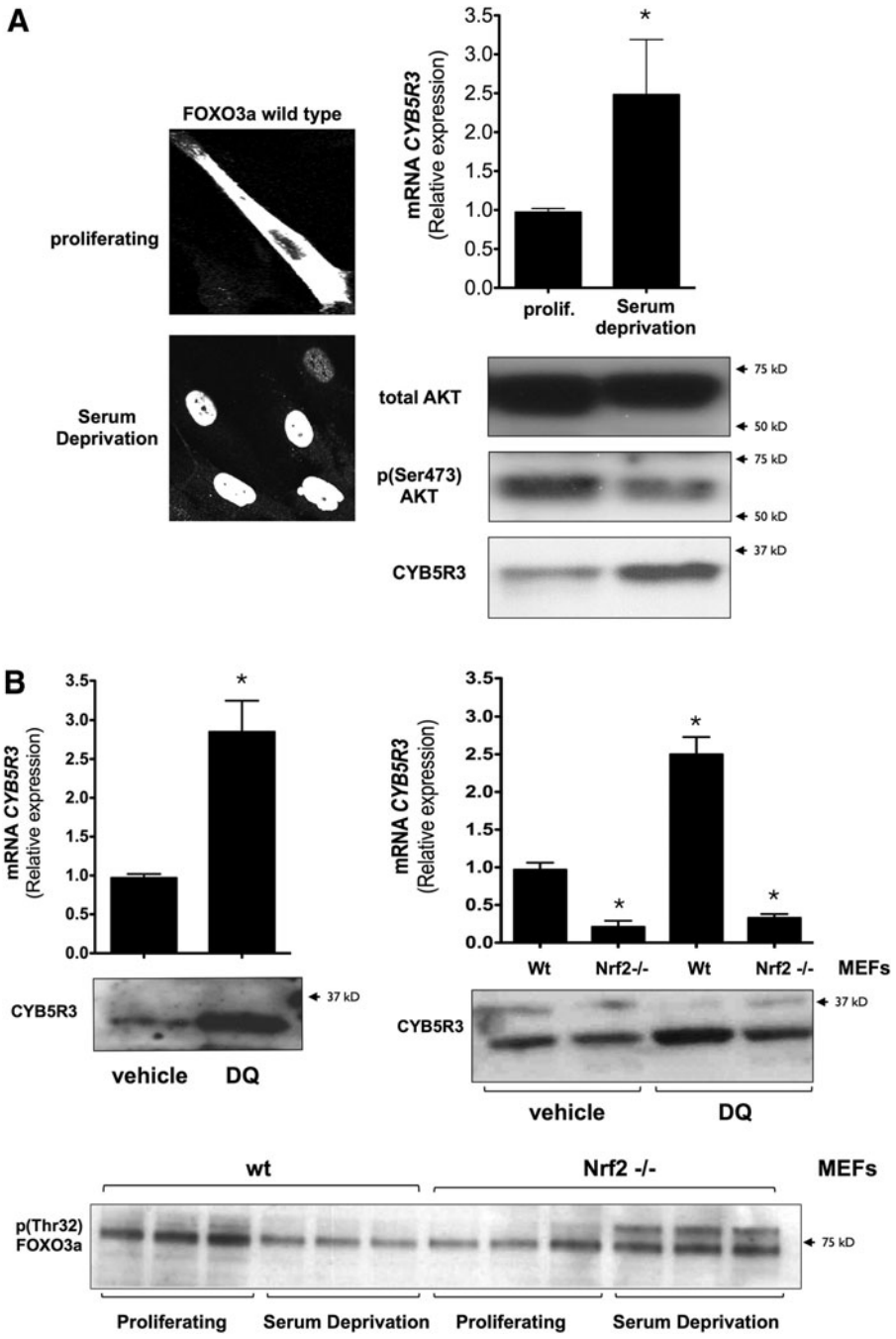

FIG. 8. CYB5R3 expression by nutritional and oxidative stress. (A) MRC-5 cells were transfected with human wild-type FOXO3a-encoding plasmid for 48 h and then cultured until confluence. After a 12-h serum deprivation, cellular distribution of recombinant FOXO3a was determined by immunofluorescence microscopy, and CYB5R3 mRNA and CYB5R3, AKT, and phospho-AKT protein expression levels were resolved. The nuclear accumulation of FOXO3a with greater expression of cytoplasmic CYB5R3 protein in response to serum deprivation should be noted. **(B)** *CYB5R3* expression in MRC-5 cells treated with DQ (100 μM) for 6 h. DMSO (vehicle)-treated cells were used as controls. Diquat stimulated CYB5R3 expression in wild-type (Wt) but not in $Nrf2^{-/-}$ MEFs. FOXO3a phosphorylation levels in proliferating and serum-deprived Wt and $Nrf2^{-/-}$ MEFs. Values are means ± SD of three different experiments. Control *versus* serum deprivation, vehicle *versus* DQ, wild-type *versus* $Nrf2^{-/-}$ MEFs, $^{*}p < 0.05$. MEF, mouse embryonic fibroblast; DQ, diquat; Nrf2, nuclear factor (erythroid-derived 2)-like2.

Our results expand *CYB5R3* functions on energy metabolism and oxidative stress protection. The PI3K/AKT pathway is activated in proliferating cells in the presence of nutrients to control cell growth, survival, and macronutrient uptake through glycolysis (4, 10). Under starvation or oxidative stress conditions, cells undergo cell cycle arrest and adapt their metabolism to these environmental conditions by a mechanism that includes the activation of FOXO3a through inactivation of the PI3K/AKT pathway (10, 11, 58). FOXO3a regulates the genes involved in cell cycle (9), mitochondrial metabolism (10, 14, 48), apoptosis (10, 16), and oxidative stress (3, 11, 14, 33). When cells undergo severe oxidative stress by exposure to electrophilic and/or oxidative chemicals, Nrf2 is released from Keap 1 and translocates to the nucleus, where it induces the expression of a large number of genes encoding cytoprotective enzymes (35, 38, 62). The promoter region of *CYB5R3* gene contains five GC box sequences upstream of the noncoding M exon, with three of them having been demonstrated to be functional and representing potential Sp1 binding sites (63). Downstream to the M exon lies binding sites for nuclear factor kappa B (NF-κB) and GATA-1 transcription factors that regulate the transcription of the soluble form of CYB5R3. Interestingly, several binding sites for Nrf2 have been identified downstream to the M exon that regulate the murine and human erythroid-soluble *CYB5R3* (29, 42). Our *in silico* study illustrated the presence of consensus ARE enhancer sequences in a 3000-bp fragment upstream of the M exon of the human *CYB5R3* gene promoter. ChIP analysis revealed the binding of Nrf2 to an ARE sequence near the transcription start site of

CYB5R3 gene (Fig. 12). The absence of FOXO3a consensus sequence in the *CYB5R3* promoter suggests that FOXO3a might not bind directly to this promoter, as evidenced by ChIP and IP assays. However, it is possible that FOXO3a binds indirectly to the *CYB5R3* promoter *via* its interaction with Nrf2. To date, the cooperation between FOXO3a and Nrf2 in humans is under debate. Data from studies carried out in *C. elegans* determined that the FOXO3a homolog, DAF-16, and the Nrf2 homolog, SKN-1, are important effectors of metabolism and longevity when the insulin/IGF signaling pathway is repressed (65). Interestingly, DAF-16 and SKN-1 had independent roles, but their target genes were common.

Consistent with these findings, it has been recently reported that the levels of *CYB5R3* protein are decreased in MEFs lacking Nrf2 gene (24). $Nrf2^{-/-}$ MEFs exhibit a lower proliferation rate when compared with wild-type MEFs and display a strong senescent phenotype. We found that *CYB5R3*-silenced MRC-5 cells and dermal fibroblasts derived from type II RHM patients exhibit reduced ability to proliferate and undergo senescence. Unfortunately, the overexpression of CYB5R3 did not completely reverse the shortening of lifespan in NRF2-KO *in vitro* (unpublished data). Nrf2 regulates the transcription of more than 200 genes, and some downstream targets of Nrf2 could play a significant role in the maintenance of normal lifespan. Thus, we consider that the lifespan shortening in $Nrf2^{-/-}$ cells might be due, in part, to lowered *CYB5R3* activity.

Intracellular NAD^+/NADH ratio has a critical role in the promotion of longevity (30, 41). Moreover, NAD^+ acts as a key modulator of longevity-associated cellular metabolism *via* FOXO signaling (36), Increased NAD^+ levels have also been associated with neuroprotection (31, 32). The genetic activation of Nrf2 correlates with increases in mitochondrial respiration rate, mitochondrial homeostasis, and energy metabolism through the availability and use of substrates, such as NADH and FADH2, of the mitochondrial electron transport chain (20). Conversely, the knockdown of Nrf2 leads to reduced mitochondrial respiration in MEFs (20). Thus, impairment in CYB5R3 expression and/or activity may result in not only NADH accumulation but also defects in mitochondrial respiration due to increased oxidative damage, ultimately leading to senescence. We propose that CYB5R3 has a key role in the maintenance of efficient aerobic metabolism in aged mammals, similar to *NQR1* orthologue in yeast (23).

Our findings indicate that CYB5R3 gene expression is induced by FOXO3a and Nrf2 in a cooperative fashion as a mechanism which adapts to starvation and promotes oxidative stress resistance. In addition, it would appear that *CYB5R3* activity plays a novel role in the control of aerobic metabolism and cytosolic NAD^+/NADH ratio, whose downregulation could be the cause of neurological disorders which are associated to type II MHR. We believe that the maintenance of cellular homeostasis by CYB5R3 requires activation

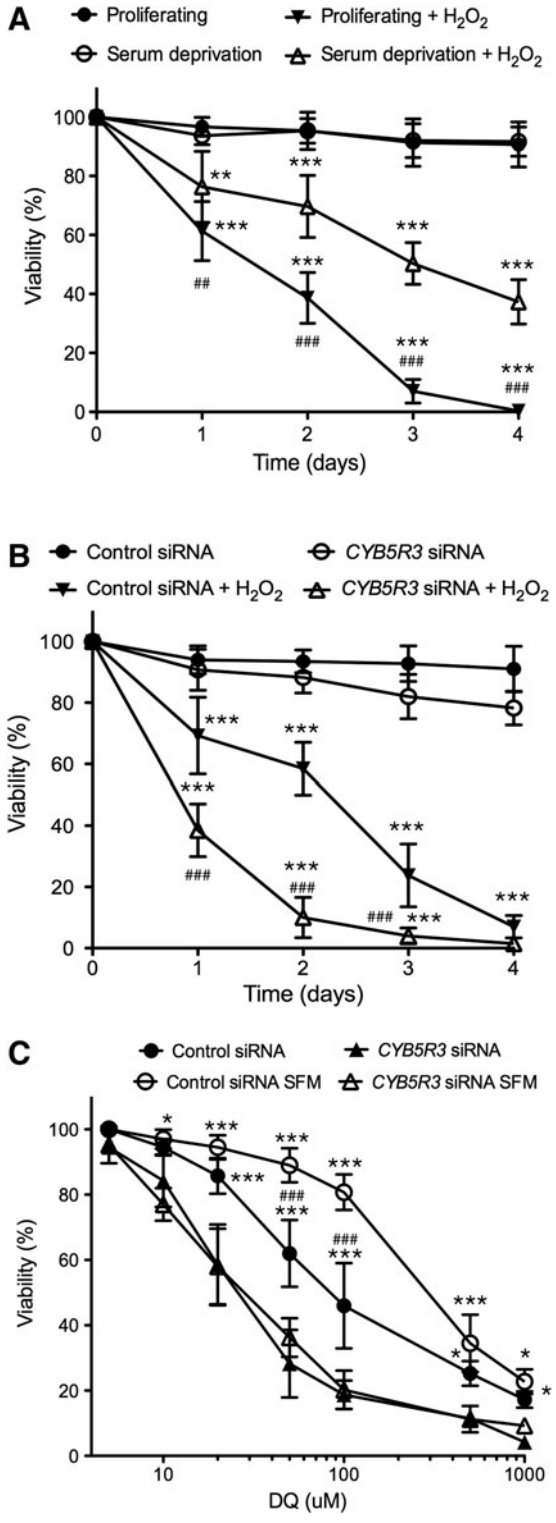

FIG. 9. Survival of MRC-5 cells exposed to oxidative stress by H_2O_2 or DQ. (A) Viability curves of proliferating and serum-deprived MRC-5 cells exposed to 75 μM of H_2O_2 for 1–4 days. **(B)** Viability curves of MRC-5 cells transfected with control and *CYB5R3* siRNAs and then exposed to 75 μM of H_2O_2 for 1–4 days. **(C)** MRC-5 cells transfected with control and *CYB5R3* siRNAs were maintained in complete medium (proliferating) or SFM and then exposed to increasing concentrations of DQ for 24 h. Viability curves were then determined. Values are means ± SD of at least three independent experiments. Untreated *versus* H_2O_2-treated cells, $^{**}p < 0.01$, $^{***}p < 0.001$. Proliferating *versus* serum-deprived cells treated with H_2O_2, $^{\#\#}p < 0.01$, $^{\#\#\#}p < 0.001$. Cells transfected with control siRNA *versus CYB5R3* siRNA and then treated with H_2O_2. $^{\#\#\#}p < 0.001$. Control siRNA *versus CYB5R3* siRNA, $^{*}p < 0.05$, $^{***}p < 0.001$. Proliferating *versus* serum-deprived cells, $^{\#\#\#}p < 0.001$. H_2O_2, hydrogen peroxide.

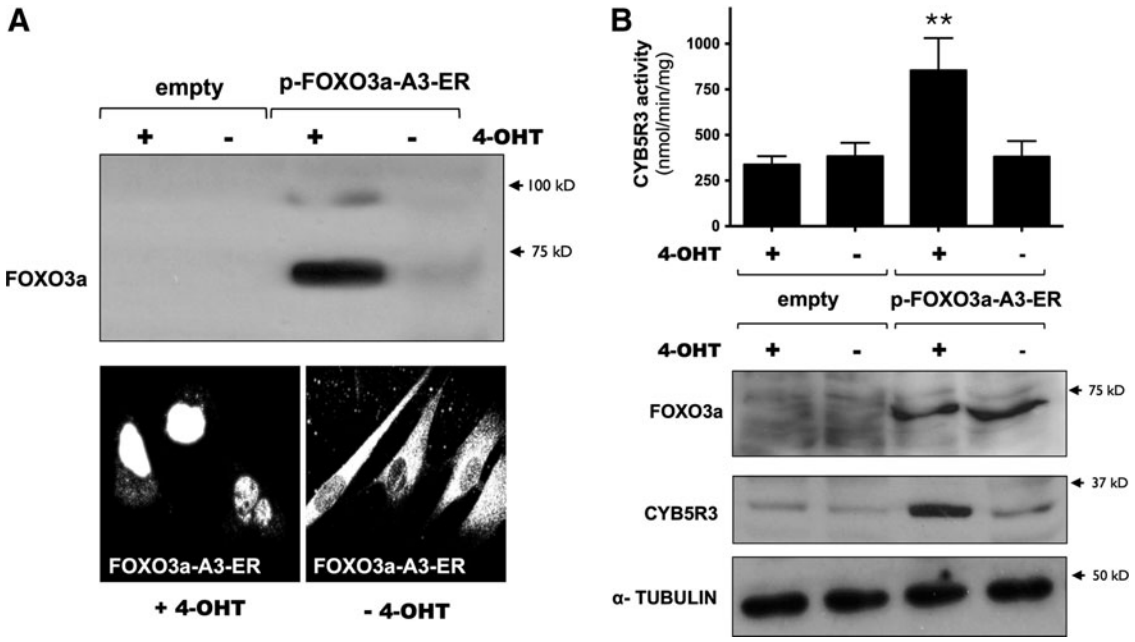

FIG. 10. Nuclear recruitment of FOXO3a is associated with cytoplasmic accumulation of active CYB5R3. MRC-5 cells were transfected with expression plasmids encoding human FOXO3a mutant fused with the ligand-binding domain of estrogen receptor (p-FOXO3a-A3-ER). Control transfection was carried out with empty plasmid. **(A)** Nuclear localization of activated FOXO3a was determined by western blot and immunofluorescence after a 24-h stimulation with 4-OHT (100 n*M*). **(B)** Enzymatic activity of CYB5R3 and immunoblot analysis of CYB5R3 and FOXO3a was performed in cytoplasmic fractions. Membranes were reprobed for α-TUBULIN, which was used as a loading control. Means ± SD of at least three different experiments are represented. $^{**}p < 0.001$. 4-OHT, 4-hydroxytamoxifen.

of the FOXO3a•Nrf2/ARE complex and further enhances the transcriptional activation of key regulators of aerobic metabolism and stress resistance which are associated with longevity. Thus, *CYB5R3* might be a promising target in the development of novel therapies for the treatment of disorders that are associated with energy depletion and oxidative stress.

Materials and Methods

All chemicals used in this study were obtained from Sigma-Aldrich, unless stated otherwise.

Cells

Primary human fibroblasts MRC-5 (CCL-171; ATCC) and neonatal HDFs (PCS-210-010 and PCS-210-012; ATCC) were cultured in Dulbecco's modified essential medium (DMEM) that was supplemented with 10% bovine serum, 10,000 U/ml penicillin, 10 mg/ml streptomycin, 25 μg/ml amphotericin B, 2 m*M* L-glutamine, and 1 g/L glucose (supplemented medium). Cells were cultured in a humidified incubator at 37°C and 5% CO_2, and detached by trypsinization at nearly confluence. Human cervical cancer cells HeLa (ATCC) and the hepatoma cells HepG2 (ATCC) were cultured in supplemented medium that was modified with 4.5 g/L glucose. MRC-5 cells were seeded at 3000 cells/cm^2 and passaged every 3–4 days. PD time of MRC-5 cells at each passage was calculated with the formula PD = log (Nf/Ni)/log2, where Nf is the final number of cells after the passage and Ni is the initial number of cells seeded. Viability of cells was estimated by the trypan blue exclusion assay after the release of cells from culture dishes using a Trypsin–EDTA solution.

MEFs preparation from wild-type and Nrf2$^{-/-}$ mice

Colonies of wild-type (Wt) and Nrf2$^{-/-}$ mice were maintained at the Translational Gerontology Branch (National Institute of Aging; National Institutes of Health). Mice were cared for in accordance to the National Institutes of Health ACUC guidelines. MEFs were obtained from fetuses at day 13 postcoitum. Pregnant female mice were sacrificed by cervical dislocation, and the uterus was dissected, rapidly washed in 70% ethanol, and placed in Hank's saline solution. Each embryo was separated from its placenta and surrounding membranes, and brain and dark red organs were also discarded. After washing, the embryos were finely minced and incubated in Trypsin–EDTA solution. Non-disaggregated tissue was removed, and the cellular suspension was washed with two volumes of fresh culture medium. After centrifugation and resuspension of the cell pellet in supplemented DMEM, cells from each embryo were seeded in 10-cm diameter dishes. The medium was changed after 24 h. Cellular confluence was obtained after a few days. Cells were then frozen and stored in liquid nitrogen. After thawing, cells were cultured in supplemented DMEM at 37°C in a humidified atmosphere of 5% CO_2 and 95% air.

NAD$^+$ and NADH measurement

NAD$^+$ and NADH levels were quantified with a commercially available kit (BioVision) according to the manufacturer's instructions. In brief, cells were lysed by two freeze/thaw cycles. To determine only NADH, samples were heated to 60°C for 30 min to decompose NAD$^+$. For the

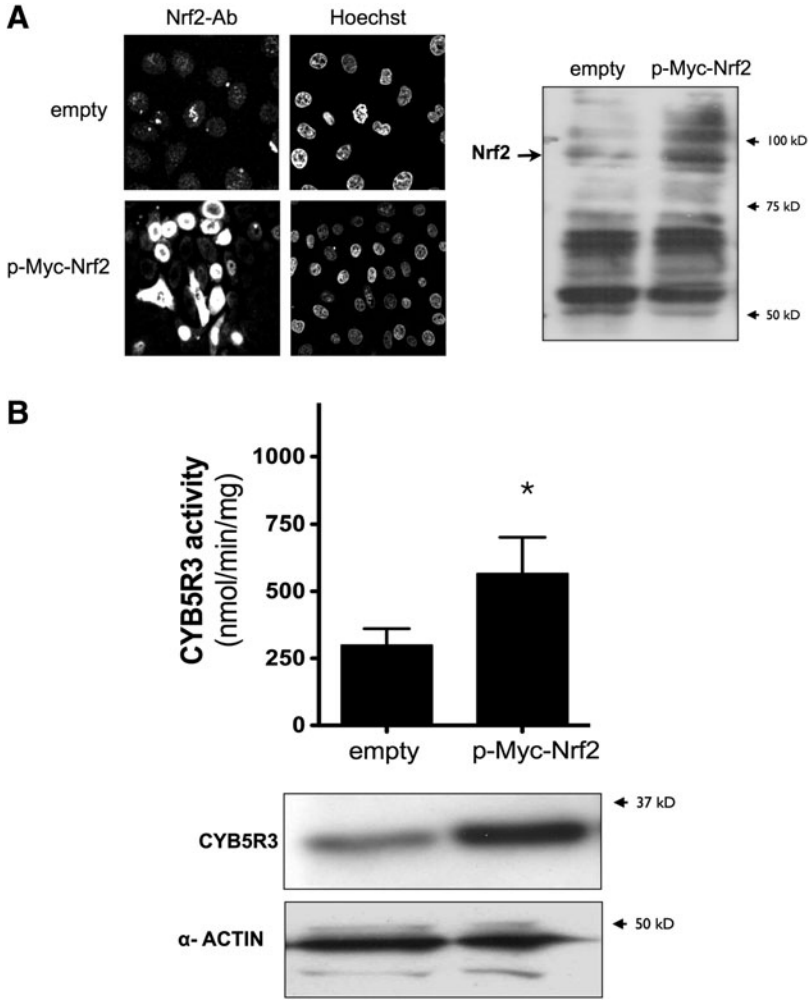

FIG. 11. Nuclear recruitment of Nrf2 is associated with cytoplasmic accumulation of active CYB5R3. (A) After 48 h of transfection, nuclear localization of human myc-tagged wild-type Nrf2 (p-Myc-Nrf2) was determined by immunofluorescence and western blot in whole cell fractions. **(B)** Cytoplasmic fractions were prepared and immunoblotted with antibodies that were raised against CYB5R3. Membranes were reprobed for α-ACTIN, which was used as a loading control. Endogenous CYB5R3 activity was also assessed in both series of experiments. Values are means ± SD of at least three different experiments. $*p < 0.05$.

detection of total NAD, samples were incubated with the NAD cycling enzyme mix (cycling buffer and enzyme) to convert NAD^+ to NADH. Both samples were then mixed with NADH developer and incubated at room temperature for 1 h before colorimetric reading absorbance at 450 nm. The amount of NAD^+ in samples was calculated by subtracting NADH from total NAD.

Quantitative real-time PCR

Total RNA was isolated with the TriPure Isolation Reagent (Roche), treated for DNA removal with deoxyribonuclease I (Sigma-Aldrich), and reverse transcribed by using the iScript cDNA Synthesis Kit (Bio-Rad). Real-time quantitative PCR was performed to measure the expression of select target genes. The reactions were carried out with iQ SYBR Green Supermix (Bio-Rad) and MyiQ™ Single-Color Real-Time PCR Detection System (Bio-Rad) on a Bio-Rad conventional thermocycler. The primers were designed with the Beacon Designer software, and the primer pair sequences used in this study were as follows: human *CYB5R*3, forward primer 5′-CCACCATGGGGGCCCAGCT-3′ and reverse primer 5′-GCGCCGGGTGTCATGGCT-3′; mouse *Cyb5r3*, forward primer 5′-CCACCATGGGGGCCCAGCT-3′ and reverse primer 5′-GGAAGCGCCGAGTGTCAGG-3′; human *NAMPT*, forward primer 5′-GCTGCCACCTTATCTTAGAGTTAT-3′ and reverse primer 5′-ACCAGAACCGAAGGCAATA-3′; human *GAPDH*, forward primer 5′-TGCACACCACCA ACTGCTTAGC-3′ and reverse primer 5′-GGCATGGAC TGTGGTCATGAG-3′; and mouse *Gapdh*, forward primer 5′-TGACGTGCCGCCTGGAGAAA-3′ and reverse primer 5′-AGTGTAGCCCAAGATGCCCTTCAG-3′. Amplification was carried on with the following thermal conditions: 30 s at 95°C and 35 cycles of 30 s at 94°C, 30 s at 60°C, and 30 s at 72°C. Fidelity of the PCR was determined by a melting curve analysis and visualization on agarose gel. Negative controls containing water instead of RNA were run to confirm that the samples were not cross-contaminated. Efficiency (E) of the PCR was determined using a dilution series, and the data were analyzed using the formula ($E_{TARGET}{}^{-CT}$/$E_{HOUSEKEEPING}{}^{-CT}$) with *GAPDH* and *Gapdh* as housekeeping genes. Each PCR was carried out with three or more biological replicates in each group.

SA-β-gal staining

SA-*β*-gal staining was used as a positive marker of senescence. Briefly, cells were cultured in six-well plates, washed with sterile phosphate-buffered saline (PBS), and then fixed in 2% formaldehyde/0.2% glutaraldehyde. After

-2344 AGTCCCAGCCACTAGGGAAGCTGAGGCAGGAGAATCGCTTGAACCCCGGAGGTTGCAGTGAGCCGCGATTGCAGTGAGCCTGGCAACAGAGCAAGACTCCGT
-2242 CTCAAAAAAGAAAAACCAACCAACCAACCAAACAAACAAAAAAAAACAGTAGGTCAGGTGGGTGGGTAGGCAGACGGGCATGGTGGCTCATGCCTGTAATCCCA
-2139 GTGCTCCGGGAGGCTGTGGTGGGAGGATGGCTTGAGCTGCAGTGAGCTGTGACTGCATCACTACACTCCAGCCTGGGCATCAGAGCGAGATCTCTTCTCTGGGT
-2035 AAATAAACCCAGTGAGTCACTCCCTCAGCTACCTAGATCCTGCAGGGCTCCCCATTCTCCTTGACATTCCAGTTCTTTCCACCCGGGGCTCCACATTGCCTCCCCAA
-1928 CGTCACATCACACCCCAGCTCGGCTGTATCAGCCCCTCTAACCTTGCCCATCAGGCCTCTGTTCACCTGTCTCCACCTCCAGGCCCTGCCAGCAAGGCGCTTCTCCC
-1821 TTTCTCTGCCTGGTCTGTGCCACGTTGCCTGAACACACAGCCCACCCCATCCCCTCAGAGCACCAGGAGCTCACATCTGGGTCCAAGACCCTACCAGGAGAGCAA
-1719 GGCAAGAGAATGACGCTAAGGCCCAGCATGAGCCTACACAGAGAAGGTGCCCACTGTCTGTCAAATTCATCCATTCAACAAGTATTTAGGCTGCTCATCGTGGCT
-1611 CACGCTTATAATCCCAGCACTTTGGGAGGCCAAGGTGGGAGGATGGCTTGAACCCAGGAGTTCCGGACCAGCCTGGGCAACATAGTGAAACCCGTCTCTACAAA
-1507 AAAATGCAAAAATGGCCGGGCGCGGTAGTTCCCACCTGTAATCCCGGCACTTTGGGAAGCCGAGGCAGGTGGATCACCTGAGGTCGGAAGTTCGAGACCAGCC
-1404 TCACCAACATGTTGAAACACCGTCTCTACTAAAAATACAAAATTAGGCCGGGCGCGGTGGCTCACGCCTGTAATCCCAGCACTTTGGGAGGCCGAGGCGGGCGG
-1300 ATCACGAGGTCAGGAGATCGAGACCATCCTCGCTAACACGGTGAAACCCCGTCCCTACTGAAAATACAAAAAATTAGCCGGGCGCGGTGGGGTGCCTGTAGTGC
-1196 CAGCTACTCGGGAGGCTGAGAATGGCGTGAACCCTGGAGGCGGAGCTTGCATTGAGCCGAAATGGCGCCACTGCATTCCAGCCTGGGGGACAGGGCGAGACT
-1094 CTGTCTCAAAAAAAAAAAAAAAAAAAAAAAAAAAAAAGATTAGCTGGTTAGCCAGATGTGGTGGCACATGCCTGTAATTTCGGGAGGCTGAGGCAGGAGGATCT
-991 GTTGAACCCTGGAGGCGGAGTTTGCGGTGAGCCGAGATCGCGTCAATGCATACCAGCCTGGGCAACAAGAGCGAAACTGCGTCTCAAAAAAAAAAACAATTAG
-888 CCGGACGTGGTGGCATGTGCCCAGCTACTCAGGAGGTTGAGGCAGGAGGAACACTTGAGCCTGGGAGGTTGAGGCTAAAGTGAGCTGTGATCAGGCTCCTGC
-786 ATTCCAGTCTGGGCAAGAGTGAGACCCTGCTTTACCAAAAAAAAAAAAAAAAAAAAAAAGGTATTTATTGAGCACCTACTATATGCTAGGCTCTGTGTGGCTAGGCT
-681 CTGGGGATGTACGGGACTTCAAACCAGATAGGGCCTTGCCCTCCGGGAGCGCACAGTCCACTGGGATGGGGTGGGAGTGGGGGAAACACGCAGGAGGCCTTC
-579 AGCTAAGTGGGACAAAGATCACTCCACAGTGGGACAATGGCGTGGGGAGCGGAGGCGCCGCCGGCGAGGAGGCTCCGGGCGGGCCGTGCTGAGACCGCAG
-479 CATTTAACCCGGCCCGAGGCAGCTGGGAACAGTGCTGCCCAGGGAACTACAAATTCAAAGGCCCGGGGAAGGGCCGCGCTGAGCAGCTGCAGGCACAGGCC
-377 CAGGCCAGGCCAGGCAGGACCGGCCCCTGCAGTCTCGGAGGCCGGGGGAAGATTCCGCCTCTTATTCTCGCTCCCATCCGGGGGGCGCCATCTTGCTTCCTTTA
-270 TGGCGGCGAACGAGGCCCAGAGAGGCCACCGTCCCGCGCGGGGCAGCACAGCGGCGGGAGAGCTCGGAGCGCAGAGGGCCGCATCCCCAGTTCCCAGTCTC
-172 CATCCCCGGCAGAAGCAGGCGGAGCGACCCGGTCCCCGCCCCCGCGCCCGCCCCCGCCCCGCGCGCCCGCCTGGCCCCTCGGCCCCGCCCCTGCTCCGGAGTGA
- 69 CGCGGGCCCGGGCGCGACGGTCTCGGCGGCGGCGGCGGCGGCGACAGAGCGAGCGCGGCGCGGGGCCACCATGGGGGCCCAGCTCAGCACGGTAGGCGG
+ 31 GGAGGGGGCGCCGGGGCCGCGGGGCGTCGCGAGGGACTGGGA

Site 1 (183 pb)
Site 2 (93 pb)

FIG. 12. Nucleotide sequence of the 5′-flanking region of the human CYB5R3 gene. *Shaded boxes* indicate putative Nrf2 binding sites. *Arrows* and *letters* in bold indicate pairs of primer sequences used to identify positive binding of Nrf2 to sites 1 and 2 on the CYB5R3 promoter region. *Underlined letters* indicate the number of base pairs of the PCR products.

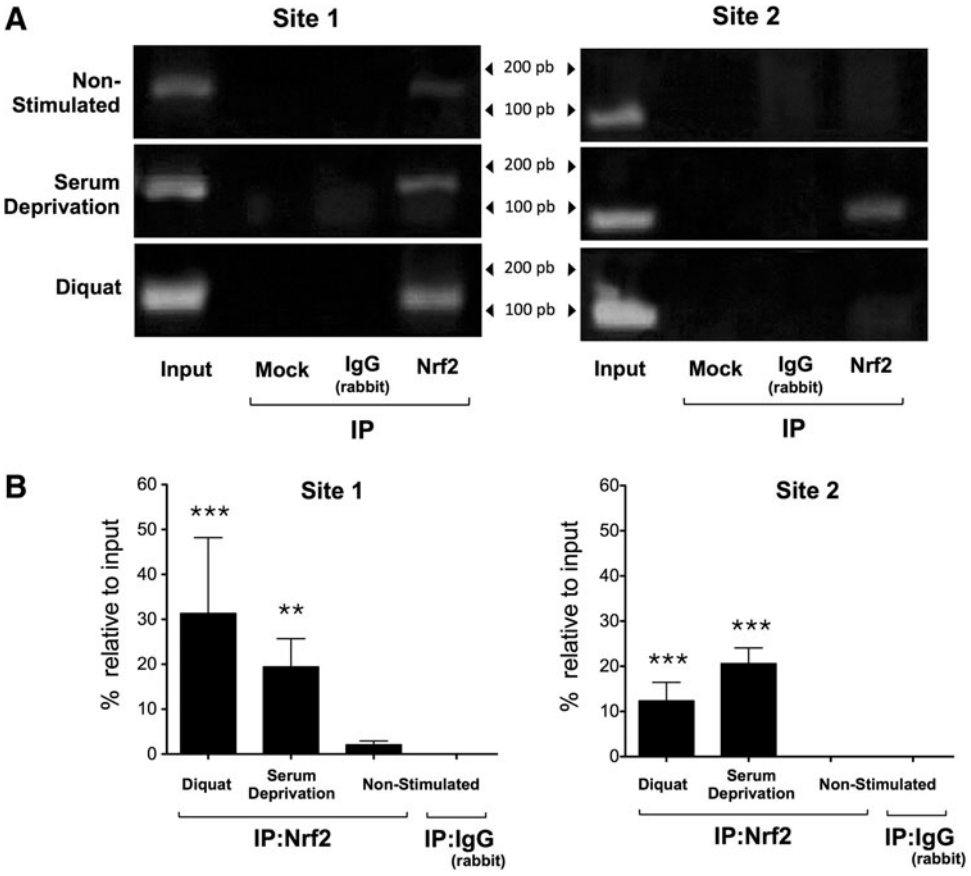

FIG. 13. Binding of Nrf2 to the promoter region of CYB5R3 gene. (A) MRC-5 cells were treated in the presence or absence of either DQ or serum deprivation for 12 h, and then, chromatin was prepared for immunoprecipitation with anti-Nrf2 for chromatin immunoprecipitation assays. Input DNA and negative controls, including chromatin samples undergoing immunoprecipitation without antibody (mock) and with nonimmune rabbit IgG, were present during semi-quantitative PCR analysis. **(B)** Results of the real-time PCR are presented as a percentage relative to input value. The experiments were repeated at least twice with similar results. Diquat and serum deprivation *versus* nonstimulated cells, $^{**}p < 0.01$, $^{***}p < 0.001$.

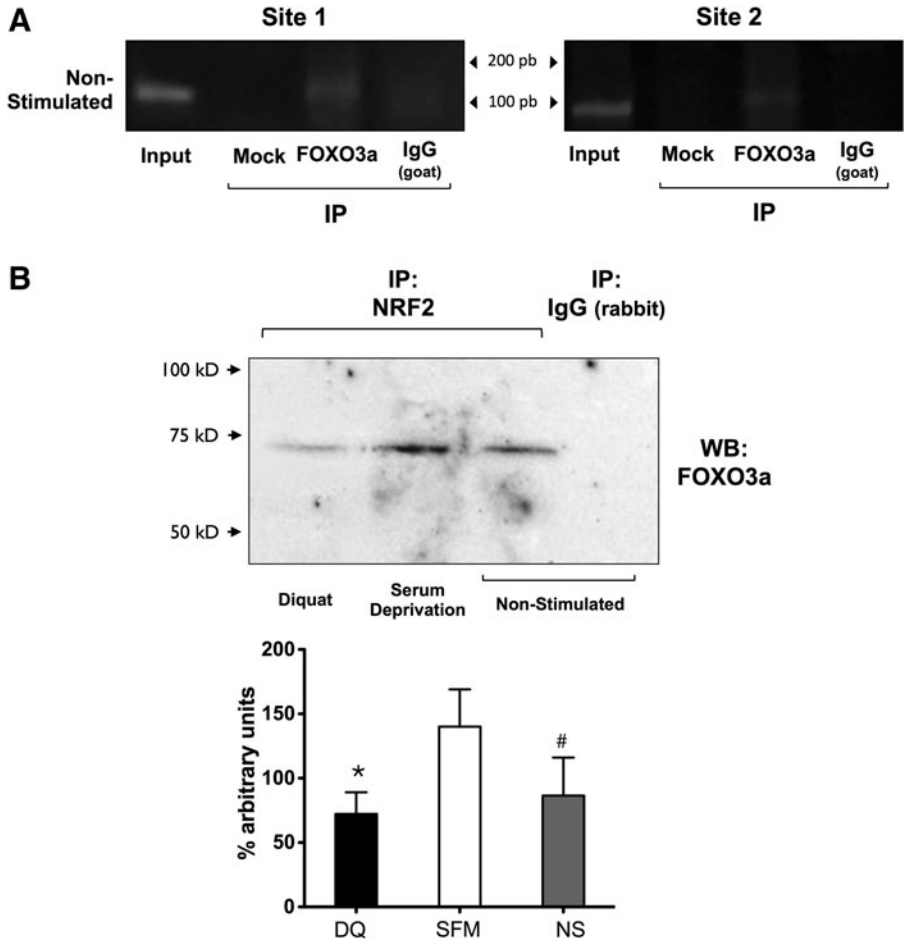

FIG. 14. Binding of FOXO3a to the promoter region of CYB5R3 gene. (A) Chromatin preparations of unstimulated MRC-5 cells were subjected to immunoprecipitation using goat anti-FOXO3a. Input DNA and negative controls, including chromatin samples undergoing immunoprecipitation without antibody (mock) and with nonimmune rabbit IgG, were included. Shown are the results of a semiquantitative PCR analysis. **(B)** MRC-5 cells were treated in the absence (NS) or presence of either DQ or serum deprivation (SFM) for 12 h. Cell lysates were immunoprecipitated with anti-Nrf2 or control rabbit IgG and then immunoblotted using anti-FOXO3a antibody (*upper panel*). *Bottom panel*, bars represent densitometric analysis of FOXO3a bands. The experiments were repeated at least twice with similar results. Serum deprivation *versus* DQ, $*p < 0.01$. Serum deprivation *versus* nonstimulated cells, $^{\#}p = 0.05$.

the fixation step, cells were incubated with staining solution (1 mg/ml X-Gal, 5 m*M* $K_3[Fe(CN)_6]$, 5 m*M* $K_4[Fe(CN)_6]$. $3H_2O$, 2 m*M* $MgCl_2$, and 150 m*M* NaCl in 40 m*M* citric acid/sodium phosphate, pH 6.0) for 4 h at 37° C. Cells were then observed under a phase-contrast microscope and photographed. Quantification of positively stained cells was carried out on micrographs.

Preparation of cell extracts for Western blot analysis

Cells were washed twice in PBS and lysed on ice for 10 min in NP-40 lysis buffer: 10 m*M* HEPES (pH 7.9), 10 m*M* KCl, 0.1 m*M* EGTA, 0.1 m*M* EDTA, 0.6% NP-40, 1 m*M* sodium orthovanadate, 1 m*M* dithiothreitol, 25 m*M* β-glycerophosphate, 0.5 m*M* phenylmethylsulfonyl fluoride, and 1 × of protease inhibitor cocktail (Sigma-Aldrich). Samples were pelleted by centrifugation at 2000 *g* for 10 min at 4°C. Supernatants (cytoplasmic extracts) were recovered and frozen at −80°C until they were used. The pellets containing the nuclear fraction were resuspended in hypertonic nuclear extraction buffer: 20 m*M* HEPES (pH 7.9), 0.4M NaCl, 1 m*M* EDTA, 1 m*M* EGTA, 1 m*M* DTT, 1 m*M* phenylmethylsulfonyl fluoride, and PIC. Cytoplasmic and nuclear proteins (25–50 μg) were separated by SDS-PAGE under reducing conditions, electrotransferred onto nitrocellulose membranes, and immunoblotted according to standard protocols. After a blocking step, membranes were incubated with the appropriate primary antibodies, followed by the addition of HRP-conjugated secondary antibodies. The detection of immunoreactive bands was performed by chemiluminescence using the ECL Western Blotting Detection System from Amersham Biosciences. Density of the protein bands was analyzed by densitometry using Image Lab 4.0.1 software from Bio-Rad. Primary antibodies used in this study were raised against CYB5R3 (37), FOXO3a (sc-9813), phospho-Thr32 FOXO3a (sc-12357), Nrf2 (sc-722), AKT (sc-81434), phospho-Ser473 AKT (sc-135651), α-tubulin (sc-8035), and α-actin (G12). All antibodies were purchased from Santa Cruz Biotechnology, Inc. with the exception of anti-CYB5R3.

Immunocytochemistry

Cells were grown on 1-mm-width glass coverslips for 48 h in DMEM, after which they were rinsed once with PBS, fixed in 3.8% paraformaldehyde for 5 min at room temperature, and then permeabilized in 0.1% saponin for 5 min. After the fixation step, glass coverslips were incubated with mouse IgG control (1:100) in PBS for 30 min at room temperature and afterward with goat anti-FOXO3a antibody (1:100) or with rabbit anti-Nrf2 (1:100) in PBS for 1 h at 37°C. After washing, FITC-labeled mouse anti-goat antibody (Calbiochem-Merck) (1:100 dilution) was added and the coverslip was incubated for 1 h at 37°C. The coverslips were then rinsed

with PBS, incubated with PBS containing Hoechst 33342 (1 μg/ml) for 1 min, and washed thrice with PBS. Finally, the coverslips were mounted onto microscope slides using Vectashield Mounting Medium (Vector Laboratories) and analyzed using an upright fluorescence microscope (Leica DMRE; Leica Microsystems).

CYB5R3 activity

Cells were lysed in isotonic buffer (130 m*M* Tris-HCl [pH 7.6], 0.1 m*M* dithiothreitol, 0.5 m*M* phenylmethylsulfonyl fluoride, and 1× of protease inhibitor cocktail [Sigma-Aldrich]) by homogenization with a micropestle. Samples were centrifuged at 2000 *g* for 10 min at 4°C, and supernatants were used to measure NADH-ferricyanide reductase activity. Thirty micrograms of protein were assayed by measuring the decrease in absorbance at 340 nm in assay medium containing 1 m*M* Tris-HCl (pH 7.6), 0.5 m*M* EDTA, and 2 m*M* potassium ferricyanide as an electron acceptor, and 0.25 m*M* NADH as an electron donor. The reaction was started by the addition of NADH. An extinction coefficient of 6.22 $mM^{-1}.cm^{-1}$ was used for calculations of specific activities.

Mitochondrial respiratory chain enzyme activities

Activities of NADH:coenzyme Q1 oxidoreductase (complex I), succinate dehydrogenase (complex II), ubiquinol: cytochrome c oxidoreductase (complex III), NADH:cytochrome c reductase (complex I–III), succinate:cytochrome c reductase (complex II–III), cytochrome c oxidase (complex IV), and citrate synthase (CS) were determined in fibroblast lysates by spectrophotometric assays as described (61). Results from mitocondrial electron transport chain activities were normalized to CS activity.

Determination of cyanide-sensitive oxygen consumption and OCRs

Mitochondrial respiration was monitored using a Clark-type oxygen electrode (YSI 5300A Biological Oxygen Monitor). All measurements were carried out at 37°C using 5×10^6 cells in air-saturated DMEM. Ten minutes after the start of the experiment, 1 m*M* potassium cyanide was added to suppress complex IV activity, which enables the measure of mitochondrial respiration through complex IV-dependent oxygen consumption.

Cellular OCRs were determined in an XF24 Extracellular Flux Analyzer (Seahorse Bioscience). Cells were plated on XF24 microplates (Seahorse Bioscience) at 15,000 cells/well in supplemented medium and incubated at 37°C and 5% CO_2 for 24 h. After the measure of BR rate, 6 μM oligomycin A was added to inhibit complex V, which was followed by the addition of 0.75 m*M* 2,4-dinitrophenol to uncouple respiration. Finally, 1 μM rotenone and 1 μM antimycin A were added to inhibit complexes I and III, respectively. Mitochondrial OCR was determined by subtracting the number of mitochondrial OCR after treatment with rotenone + antimycin A. Mitochondrial BR was determined from mitochondrial OCR before the administration of oligomycin. Mitochondrial maximal respiration was mitochondrial OCR after 2,4-dinitrophenol administration. SRC was mitochondrial maximal respiration minus mitochondrial BR.

Determination of lactate levels and ATP levels

Cells were seeded on a 24-well microplate and grown during 24 h. Medium was collected and lactate was determined by using the colorimetric lactate oxidase-peroxidase assay lactate kit (Spinreact) as indicated by the manufacturer. The concentration of lactate in the medium was determined by a comparison with the signal obtained from a standard with a known amount of lactate provided by the manufacturer. The amount determined in the medium without cells was also determined and subtracted from the amount determined in the presence of cells.

ATP levels in cells were determined by using the Cell Titer-Glo Luminiscent assay (Promega) as determined by the manufacturer. Briefly, the same amount of reactive solution was added to culture medium and left to produce cell lysis with a gentle movement. The mixture was homogenized and transferred to a white polystyrene 96-well assay plate. A patron with known amounts of ATP was also added in the same plate and mixed with reactive solution in a 1:1 proportion. Luminiscence was determined by using a POLAR Star Omega fluorimeter (BMG Labtech) and analyzed with the Omega Data Analysis software (BMG Labtech). The ATP amount referred to the total amount of cells counted by a hemocytometer after trypsine detachment and that were seeded in a 24-well plate in parallel.

Plasmids and transfection

The Flag-FOXO3a-wt (Plasmid No. 8360), HA-FOXO3a-A3 mutant (Plasmid No. 1788), and HA-FOXO3a-A3-ER mutant (Plasmid No. 8353), created by Greenberg and coworkers (8, 64), pCDNA3-Myc3-Nrf2, created by Y Xiong (17) (Plasmid No. 21555), and pcDNA3-Myr-HA-Akt1, created by Ramaswamy *et al.* (51) (Plasmid No. 1036), were obtained from Addgene. The Flag-FOXO1-A3 and Flag-FOXO4-A3 mutants were a generous gift from Dr. Agustín Hernández (Universidad Pablo de Olavide, Sevilla, Spain). Briefly, the day before transfection, cells were seeded in DMEM that was supplemented with 5% serum without antibiotics. One hour before transfection, the medium was replaced with fresh medium. One hour before transfection, the medium was changed. For each single transfection, lipofectamine reagent was diluted in OPTIMEM media (Invitrogen) and incubated for 10 min at room temperature. Plasmids were added to the diluted transfection reagent mixture and further incubated for 30 min at room temperature. Then, the transfection complex was added to the cells.

SiRNA, ShRNA, transfections and infections

SiRNAs targeting the *CYB5R3* were acquired from Ambion (AM16708A Silencer predesigned siRNA No. 8546, No. 110649, No. 110650). Cells were transfected with oligofectamine (Invitrogen), following the manufacturer's instructions. Briefly, the day before transfection, cells were plated in DMEM 5% serum without antibiotics. One hour before transfection, media were changed. For each single transfection, oligofectamine reagent was diluted in OPTI-MEM media (Invitrogen) and incubated for 10 min at room temperature. SiRNA mix was added to the diluted transfection reagent mixture and further incubated for 30 min at

room temperature. Then, the transfection complex was added to the cells.

Lentiviral particles and shRNA of *CYB5R3* (sc-62173-V) incorporated into lentivirus were purchased from Santa Cruz Biotechnology. The lentiviral particles contained three to five expression constructs with each encoding target-specific 19–25 nt (plus hairpin) shRNA designed for silencing *CYB5R3* expression. Cells were plated in a six-well plate at 5000 cells/well in supplemented medium at 24 h before viral infection. Media were removed from plate wells and replaced with supplemental medium with Polybrene® (sc-134220) at a final concentration of 5 μg/ml. Next, cells were infected by adding shRNA lentiviral particles to the culture. Stable clones expressing the shRNA were selected *via* puromycin dihydrochloride.

ChIP analysis

Chromatin protein DNA of cells was fixed (cross-linked) in neutral-buffered 1% formaldehyde at room temperature for 10 min. Further fixation was stopped by the addition of 125 m*M* glycine buffer. DNA was sheared by sonication on ice into fragments of 500 bp. An aliquot of sample supernatant was saved as input DNA for PCR analysis. After preclearing with protein A agarose beads, supernatants were incubated with a ChIP-graded anti-Nrf2 antibody (sc-722X; Santa Cruz) or an anti-FOXO3 antibody (sc-9813; Santa Cruz) in rotation at 4°C overnight. To control for nonspecific binding of the antibody used, an equal amount of the IgG host antibody was included in a separate batch of control supernatants and followed through the remaining protocols. Antibody-chromatin complexes were collected, and DNA was released from cross-linked complexes with proteinase K at 65°C for 4 h followed by 72°C for 10 min. DNA was then extracted and eluted with 120 μl of Tris, pH 8.0, buffer using the DNeasy kit (Qiagen), and the contaminant RNA was cleaved with RNase A (Invitrogen). The detection of positive fragments was carried out by standard and real-time PCR using the primers described in Figure 6A.

Nrf2/ARE pathway activity assay and MTT assay

ARE-*bla* HepG2 cells (purchased from Invitrogen) were seeded at a density of 35,000 cells/well in white-walled 96-well tissue culture plates and allowed to expand until 80% confluence. Cells were treated with various concentrations of diquat or 25 μ*M* of tert-butylhydroquinone (tBHQ; Fisher) that served as a positive control, and incubated at 37°C for 4 h. After treatment, the medium was removed, and the cells were washed with 1 × PBS followed by incubation with a β-lactamase substrate (Lytic Blazer; Invitrogen) for 4 h at 37°C. Relative fluorescence values were determined at an excitation/emission wavelength of 485/530 nm in a 1420 multilabel counter (Perkin Elmer). Values for wells without treatment were subtracted from all readings. Viability of cells was determined by MTT assay. Cells were treated with diquat or tBHQ as described earlier, and medium was removed and replaced with a 0.5% MTT (3-(4,5-dimethylthiazol-2-yl)-2,5-diphenyltetrazolium bromide) solution (Sigma-Aldrich). Plates were incubated for an additional 3 h, after which the MTT solution was removed and blue formazan crystals were solubilized with 100 μl of dimethylsulfoxide (Sigma-Aldrich). Optical density was determined at 590 nm using a 96-well plate reader 1420 multilabel counter.

Statistical analysis

Significant differences between the data groups were evaluated using a paired *t*-test (two-tailed *p*-values) for comparing two groups and by two-way ANOVA for >2 groups using GraphPad Prism (GraphPad Software, Inc.). Multiple comparisons of ANOVA were followed with *post-hoc* Bonferroni. Results are expressed as the means ± SD and were considered significant at $p \leq 0.05$.

Acknowledgments

This work has been partially funded by the Spanish FIS grant (PI11/00078) and Junta de Andalucía grant P08-CTS-03988. The authors would like to thank José Manuel Cuezva and María Sánchez-Aragó for helping them with the XF24 Extracellular Flux Analyzer and the interpretation of mitochondrial consumption rate results.

Author Disclosure Statement

No competing financial interests exist.

References

1. Aguer C, Gambarotta D, Mailloux RJ, Moffat C, Dent R, McPherson R, and Harper ME. Galactose enhances oxidative metabolism and reveals mitochondrial dysfunction in human primary muscle cells. *PLoS One* 6: e28536, 2011.
2. Alejandro K. Samhan-Arias A, Garcia-Bereguiain MA, Martin-Romero FJ, and Gutierrez-Merino C. Clustering of plasma membrane-bound cytochrome b5 reductase within 'lipid raft' microdomains of the neuronal plasma membrane. *Mol Cell Neurosci* 40: 14–26, 2009.
3. Ambrogini E, Almeida M, Martin-Millan M, Paik JH, Depinho RA, Han L, Goellner J, Weinstein RS, Jilka RL, O'Brien CA, and Manolagas SC. FoxO-mediated defense against oxidative stress in osteoblasts is indispensable for skeletal homeostasis in mice. *Cell Metab* 11: 136–146, 2010.
4. Barthel A, Schmoll D, and Unterman TG. FoxO proteins in insulin action and metabolism. *Trends Endocrinol Metab* 16: 183–189, 2005.
5. This reference has been deleted.
6. This reference has been deleted.
7. Bello RI, Alcaín FJ, Gómez-Díaz C, López-Lluch G, Navas P, and Villalba JM. Hydrogen peroxide- and cell-density-regulated expression of NADH-cytochrome b_5 reductase in HeLa cells. *J Bioenerg Biomembr* 35: 169–179, 2003.
8. Brunet A, Sweeney LB, Sturgill JF, Chua KF, Greer PL, Lin Y, *et al.* Stress-dependent regulation of FOXO transcription factors by the SIRT1 deacetylase. *Science* 303: 2011–2015, 2004.
9. Burgering BM and Kops GJ. Cell cycle and death control: long live Forkheads. *Trends Biochem Sci* 27: 352–360, 2002.
10. Burgering BM and Medema RH. Decisions on life and death: FOXO Forkhead transcription factors are in command when PKB/Akt is off duty. *J Leukoc Biol* 73: 689–701, 2003.

11. Chiribau CB, Cheng L, Cucoranu IC, Yu YS, Clempus RE, and Sorescu D. FOXO3A regulates peroxiredoxin III expression in human cardiac fibroblasts. *J Biol Chem* 283: 8211–8217, 2008.
12. De Cabo R, Burgess JR, and Navas P. Adaptations to oxidative stress induced by vitamin E deficiency in rat liver. *J Bioenerg Biomembr* 38: 309–317, 2006.
13. De Cabo R, Cabello R, Rios M, Lopez-Lluch G, Ingram DK, Lane MA, and Navas P. Calorie restriction attenuates age-related alterations in the plasma membrane antioxidant system in rat liver. *Exp Gerontol* 39: 297–304, 2004.
14. de Keizer P, Burgering B, and Dansen TB. FOXO as a sensor, mediator and regulator of redox signaling. *Antioxid Redox Signal* 14: 1093–1106, 2011.
15. Ewenczyk C, Leroux A, Roubergue A, Laugel V, Afenjar A, Saudubray JM, Beauvais P, Billette de Villemeur T, Vidailhet M, and Roze E. Recessive hereditary methaemoglobinaemia, type II: delineation of the clinical spectrum. *Brain* 131: 760–771, 2008.
16. Federico A, Cardaioli E, Da Pozzo P, Formichi P, Gallus GN, and Radi E. Mitochondria, oxidative stress and neurodegeneration. *J Neurol Sci* 15: 254–262, 2012.
17. Furukawa M and Xiong Y. BTB protein Keap1 targets antioxidant transcription factor Nrf2 for ubiquitination by the Cullin 3-Roc1 ligase. *Mol Cell Biol* 25: 162–171, 2005.
18. Ge X, Zhang Y, and Jiang H. Signaling pathways mediating the effects of insulin-like growth factor-I in bovine muscle satellite cells. *Mol Cell Endocrinol* 372: 23–29, 2013.
19. Hildebrandt A and Estabrook RW. Evidence for the participation of cytochrome b_5 in hepatic microsomal mixed-function oxidation reactions. *Arch Biochem Biophys* 143: 66–79, 1971.
20. Holmström KM, Baird L, Zhang Y, Hargreaves I, Chalasani A, Land JM, Stanyer L, Yamamoto M, Dinkova-Kostova AT, and Abramov AY. Nrf2 impacts cellular bioenergetics by controlling substrate availability for mitochondrial respiration. *Biol Open* 2: 761–770, 2013.
21. Hyun DH, Emerson S, Jo DG, Mattson MP, and de Cabo R. Calorie restriction up-regulates the plasma membrane redox system in brain cells and suppresses oxidative stress during aging. *Proc Natl Acad Sci U S A* 103: 19908–19912, 2006.
22. Hyun DH, Hunt ND, Emerson SS, Hernandez JO, Mattson MP, and de Cabo R. Up-regulation of plasma membrane-associated redox activities in neuronal cells lacking functional mitochondria. *J Neurochem* 100: 1364–1374, 2007.
23. Jimenez-Hidalgo M, Santos-Ocana C, Padilla S, Villalba JM, Lopez-Lluch G, Martin-Montalvo A, Minor RK, Sinclair DA, de Cabo R, and Navas P. NQR1 controls lifespan by regulating the promotion of respiratory metabolism in yeast. *Aging Cell* 8: 140–151, 2009.
24. Jódar L, Mercken EE, Ariza J, Younts C, González-Reyes JA, Alcaín FJ, Burón I, de Cabo R, and Villalba JM. Genetic deletion of Nrf2 promotes immortalization and decreases lifespan of murine embryonic fibroblasts. *J Gerontol A Biol Sci Med Sci* 66: 247–256, 2011.
25. This reference has been deleted.
26. Kapeta S, Chondrogianni N, and Gonos ES. Nuclear erythroid factor 2-mediated proteasome activation delays senescence in human fibroblasts. *J Biol Chem* 285: 8171–8184, 2010.
27. Kops GJ, Dansen TB, Polderman PE, Saarloos I, Wirtz KW, Coffer PJ, Huang TT, Bos JL, Medema RH, and Burgering BM. Forkhead transcription factor FOXO3a protects quiescent cells from oxidative stress. *Nature* 419: 316–321, 2002.
28. Kryston TB, Georgiev AB, Pissis P, and Georgakilas AG. Role of oxidative stress and DNA damage in human carcinogenesis. *Mutat Res* 711: 193–201, 2011.
29. Leroux A, Mota Vieira L, and Kahn A. Transcriptional and translational mechanisms of cytochrome b5 reductase isoenzyme generation in humans. *Biochem J* 355: 529–535, 2001.
30. Lin SJ and Guarente L. Nicotinamide adenine dinucleotide, a metabolic regulator of transcription, longevity and disease. *Curr Opin Cell Biol* 15: 241–246, 2003.
31. Liu D, Gharavi R, Pitta M, Gleichmann M, and Mattson MP. Nicotinamide prevents NAD+ depletion and protects neurons against excitotoxicity and cerebral ischemia: NAD+ consumption by SIRT1 may endanger energetically compromised neurons. *Neuromolecular Med* 11: 28–42, 2009.
32. Liu D, Pitta M, and Mattson MP. Preventing NAD+ depletion protects neurons against excitotoxicity: bioenergetic effects of mild mitochondrial uncoupling and caloric restriction. *Ann NY Acad Sci* 1147: 275–282, 2008.
33. Marinkovic D, Zhang X, Yalcin S, Luciano JP, Brugnara C, Huber T, and Ghaffari S. Foxo3 is required for the regulation of oxidative stress in erythropoiesis. *J Clin Invest* 117: 2133–2144, 2007.
34. Marroquin LD, Hynes J, Dykens JA, Jamieson JD, and Will Y. Circumventing the Crabtree effect: replacing media glucose with galactose increases susceptibility of HepG2 cells to mitochondrial toxicants. *Toxicol Sci* 97: 539–547, 2007.
35. Martín-Montalvo A, Villalba JM, Navas P, and de Cabo R. Nrf2, cancer and calorie restriction. *Oncogene* 30: 505–520, 2011.
36. Mouchiroud L, Houtkooper RH, Moullan N, Katsyuba E, Ryu D, Cantó C, Mottis A, Jo YS, Viswanathan M, Schoonjans K, Guarente L, and Auwerx J. The NAD(+)/sirtuin pathway modulates longevity through activation of mitochondrial UPR and FOXO signaling. *Cell* 2013 154: 430–441, 2013.
37. Navarro F, Villalba JM, Crane FL, McKellar WC, and Navas P. A phospholipid-dependent NADH-coenzyme Q reductase from liver plasma membrane. *Biochem Biophys Res Commun* 212: 138–143, 1995.
38. Navas P, Villalba JM, and de Cabo R. The importance of plasma membrane coenzyme Q in aging and stress responses. *Mitochondrion* 7: S34–S40, 2007.
39. Navas P and Villalba JM. Regulation of ceramide signaling by plasma membrane coenzyme Q reductases. *Methods Enzymol* 378: 200–206, 2004.
40. Nguyen T, Nioi P, and Pickett CB. The Nrf2-antioxidant response element signaling pathway and its activation by oxidative stress *J Biol Chem* 284: 13291–13295, 2009.
41. Olgun A. Converting NADH to NAD+ by nicotinamide nucleotide transhydrogenase as a novel strategy against mitochondrial pathologies during aging. *Biogerontology* 10: 531–534, 2009.
42. Orkin S. Transcription factors and hematopoietic development. *J Biol Chem* 270: 4955–4958, 1995.
43. Osburn WO, Wakabayashi N, Misra V, Nilles T, Biswal S, Trush MA, and Kensler TW. Nrf2 regulates an adaptive

response protecting against oxidative damage following diquat-mediated formation of superoxide anion. *Arch Biochem Biophys* 454: 7–15, 2006.
44. Oshino N, Imai Y, and Sato R. A function of cytochrome b5 in fatty acid desaturation by rats liver microsomes. *J Biochem* 69: 155–167, 1971.
45. Passon PG and Hultquist DE. Soluble cytochrome b_5 reductase from human erythrocytes. *Biochim Biophys Acta* 275: 62–73, 1972.
46. Pearson KJ, Lewis KN, Price NL, Chang JW, Perez E, Cascajo MV, Tamashiro KL, Poosala S, Csiszar A, Ungvari Z, Kensler TW, Yamamoto M, Egan JM, Longo DL, Ingram DK, Navas P, and de Cabo R. Nrf2 mediates cancer protection but not prolongevity induced by caloric restriction. *Proc Natl Acad Sci U S A* 105: 2325–2330, 2008.
47. Percy MJ and Lappin TR. Recessive congenital methaemoglobinaemia: cytochrome b5 reductase deficiency. *Br J Haematol* 141: 298–308, 2008.
48. Pirinen E, Lo Sasso G, and Auwerx J. Mitochondrial sirtuins and metabolic homeostasis. *Best Prac Res Clin Endocrinol Metab* 26: 759–770, 2012.
49. Quinzii CM, López LC, Gilkerson RW, Dorado B, Coku J, Naini AB, Lagier-Tourenne C, Schuelke M, Salviati L, Carrozzo R, Santorelli F, Rahman S, Tazir M, Koenig M, DiMauro S, and Hirano M. Reactive oxygen species, oxidative stress, and cell death correlate with level of CoQ10 deficiency. *FASEB* J 24: 3733–3743, 2010.
50. Quinzii CM, López LC, Von-Moltke J, Naini A, Krishna S, Schuelke M, Salviati L, Navas P, DiMauro S, and Hirano M. Respiratory chain dysfunction and oxidative stress correlate with severity of primary CoQ10 deficiency. *FASEB J* 22: 1874–1885, 2008.
51. Ramaswamy S, Nakamura N, Vazquez F, Batt DB, Perera S, Roberts TM, and Sellers WR. Regulation of G1 progression by the PTEN tumor suppressor protein is linked to inhibition of the phosphatidylinositol 3-kinase/Akt pathway. *Proc Natl Acad Sci U S A* 96: 2110–2115, 1999.
52. Reddy MJ and Caspi KD. Mechanism of C-5 double bound introduction in the biosynthesis of cholesterol by rat liver microsomes. *J Biol Chem* 252: 2797–2801, 1997.
53. Robida-Stubbs S, Glover-Cutter K, Lamming DW, Mizunuma M, Narasimhan SD, Neumann-Haefelin E, Sabatini DM, and Blackwell TK. TOR signaling and rapamycin influence longevity by regulating SKN-1/Nrf and DAF-16/FoxO. *Cell Metab* 15: 713–724, 2012.
54. Robinson BH, Petrova-Benedict R, Buncic JR, and Wallace DC. Nonviability of cells with oxidative defects in galactose medium: a screening test for affected patient fibroblasts. *Biochem Med Metab Biol* 48: 122–126, 1992.
55. Ronnebaum SM and Patterson C. The FoxO family in cardiac function and dysfunction. *Annu Rev Physiol* 72: 81–94, 2010.
56. Rossignol R, Gilkerson R, Aggeler R, Yamagata K, Remington SJ, and Capaldi RA. Energy substrate modulates mitochondrial structure and oxidative capacity in cancer cells. *Cancer Res* 64: 985–993, 2004.
57. Sacco JC and Trepanier LA. Cytochrome b5 and NADH cytochrome b5 reductase: genotype-phenotype correlations for hydroxylamine reduction. *Pharmacogenet Genomics* 20: 26–37, 2010.
58. Salminen A and Kaarniranta K. Insulin/IGF-1 paradox of aging: regulation via AKT/IKK/NF-kappaB signaling. *Cell Signal* 22: 573–577, 2010.
59. Santo EE, Stroeken P, Sluis PV, Koster J, Versteeg R, and Westerhout EM. FOXO3a is a major target of inactivation by PI3K/AKT signaling in aggressive neuroblastoma. *Cancer Res* 73: 2189–2198, 2013.
60. Singh U and Jialal I. Oxidative stress and atherosclerosis. *Pathophysiology* 13: 129–42, 2006.
61. Spinazzi M, Casarin A, Pertegato V, Salviati L, and Angelini C. Assessment of mitochondrial respiratory chain enzymatic activities on tissues and cultured cells. *Nat Protoc* 7: 1235–1246, 2012.
62. Taguchi K, Motohashi H, and Yamamoto M. Molecular mechanisms of the Keap1–Nrf2 pathway in stress response and cancer evolution. *Genes Cells* 16: 123–140, 2011.
63. Toyoda A, Fukumaki Y, Hattori M, and Sakaki Y. Mode of activation of the GC box/Sp1-dependent promoter of the human NDH-cytochrome b5 reductase-encoding gene. *Gene* 164: 351–355, 1995.
64. Tran H, Brunet A, Grenier JM, Datta SR, Fornace AJ, Jr., DiStefano PS, Chiang LW, and Greenberg ME. DNA repair pathway stimulated by the forkhead transcription factor FOXO3a through the Gadd45 protein. *Science* 296: 530–534, 2002.
65. Tullet JMA, Hertweck M, An JH, Baker J, Oliviera RP, Baumeister R, and Blackwell TK. Direct inhibition of the longevity promoting factor SKN-1 by Insulin like signaling in *C. elegans*. *Cell* 132: 1025–1038, 2008.
66. van der Vos KE, Eliasson P, Proikas-Cezanne T, Vervoort SJ, van Boxtel R, Putker M, van Zutphen IJ, Mauthe M, Zellmer S, Pals C, Verhagen LP, Groot Koerkamp MJ, Braat AK, Dansen TB, Holstege FC, Gebhardt R, Burgering BM, and Coffer PJ. Modulation of glutamine metabolism by the PI(3)K-PKB-FOXO network regulates autophagy. *Nat Cell Biol* 14: 829–837, 2012.
67. Wong HK, Veremeyko T, Patel N, Lemere CA, Walsh DM, Esau C, Vanderburg C, and Krichevsky AM. De-repression of FOXO3a death axis by microRNA-132 and -212 causes neuronal apoptosis in Alzheimer's disease. *Hum Mol Genet* 22: 3077–3092, 2013.
68. Wu KC, Zhang Y, and Klaassen CD. Nrf2 protects against diquat-induced liver and lung injury. *Free Radic Res* 46: 1220–1229, 2012.
69. Yueping Sun IA, Lindeke C, and Moldéus P. The protective effect of sulfite on menadione- and diquat-induced cytotoxicity in isolated rat hepatocytes. *Pharmacol Toxicol* 5: 393–398, 1990.

Address correspondence to:
Dr. Plácido Navas
Centro Andaluz de Biología del Desarrollo
Universidad Pablo de Olavide
Carretera de Utrera km 1
Seville 41013
Spain

E-mail: pnavas@upo.es

Date of first submission to ARS Central, June 24, 2013; date of final revised submission, January 13, 2014; date of acceptance, January 22, 2014.

Abbreviations Used

4-OHT = 4-hydroxytamoxifen
AKT = v-akt murine thymoma viral oncogene homolog 1
ARE = antioxidant response elements
BR = basal respiration
ChIP = chromatin immunoprecipitation
CS = citrate synthase
DMEM = Dulbecco's modified essential medium
DNP = 2,5-dinitrophenol
DQ = diquat
FOXO3a = forkhead box class O 3a
GATA-1 = GATA binding protein 1 (globin transcription factor 1)
H_2O_2 = hydrogen peroxide
HDF = human dermal fibroblast
MEF = mouse embryonic fibroblast
Mit. OCR = mitochondrial oxygen consumption rates
MR = maximal respiration
NAMPT = nicotinamide phosphoribosyltransferase
NF-κB = nuclear factor kappa B
NQO1 = NAD(P)H:quinone oxidoreductase 1
NQR1 = NADH-coenzyme Q reductase 1
Nrf2 = nuclear factor (erythroid-derived 2)-like2
PBS = phosphate-buffered saline
PCR = polymerase chain reaction
PD = population doublings
PI3K = phosphatidylinositol-4,5-bisphosphate 3-kinase
RHM = recessive hereditary methaemoglobinaemia
SA-β-gal = senescence-associated β-galactosidase
SFM = serum-free medium
SP1 = sp1 transcription factor
SRC = spare respiratory capacity
tBHQ = tert-butylhydroquinone